Probing Biased Activation of mu-opioid Receptor by the Biased Agonist PZM21 Using all Atom Molecular Dynamics Simulation

Siyan Liao[1, 2], Kai Tan[2, 3], Cecilia Floyd[2], Daegun Bong[2], Michael James Pino Jr[2] and Chun Wu[2*]

[1] Key Laboratory of Molecular Target & Clinical Pharmacology, School of Pharmaceutical Sciences, Guangzhou Medical University, Guangzhou, 511436, China

[2] College of Science and Mathematics, Rowan University, Glassboro, NJ, 08028 USA

[3] Department of Chemistry, Xiamen University, Xiamen, Fujian, 361005, China

ABSTRACT

Morphine is a commonly used opioid drug to treat acute pain by binding to the mu-opioid receptor (MOR), but its effective analgesic efficacy via triggering of the heterotrimeric G_i protein pathway is accompanied by a series of adverse side effects via triggering of the β-arrestin pathway. Recently, PZM21, a recently developed MOR biased agonist, shows preferentially activating the G protein pathway over β-arrestin pathway. However, there is no high-resolution receptor structure in complex with PZM21 and its action mechanism remains elusive. In this study, PZM21 and Morphine were docked to the active human MOR-1 homology structure and then subjected to the molecular dynamics (MD) simulations in two different situations (i.e., one situation includes the crystal waters but another does not). Detailed comparisons between the two systems were made to characterize the differences in protein-ligand interactions, protein secondary and tertiary structures and dynamics networks. PZM21 could strongly interact with $Y328^{7.43}$ of TM7, besides the residues ($Asp149^{3.32}$ and $Tyr150^{3.33}$) of TM3. The two systems' network paths to the intracellular end of TM6 were roughly similar but the paths to the end of TM7 were different. The PZM21-bound MOR's intracellular ends of TM5-7 bent outward more along with the distance changes of the three key molecular switches (ionic lock, transmission and Tyr toggle) and the distance increase of some conserved inter-helical residue pairs. The larger intracellular opening of the receptor could potentially facilitate G protein binding.

Keywords: mu-opioid receptor; PZM21; molecular docking; MD simulation; network analysis

---

Abbreviations: MOR, mu-opioid receptor; MD, molecular dynamics; GPCR, G-protein-coupled receptor; TM, transmembrane; POPC, 1-palmitoyl-2-oleoyl-sn-phosphatidylcholine; SID, simulation interaction diagram; RMSD, root mean square deviation; SSE, secondary structure element; RMSF, root mean square fluctuation; C_α, alpha carbons; ICL, intracellular loop; ECL, extracellular loop; β_2AR, β_2-adrenergic receptor; HHM, hydrophobic hindering mechanism core; NMA, normal mode analysis; PCA, principal component analyses.

* Corresponding author

E-mail address: wuc@rowan.edu (Chun Wu).

1. Introduction

Opioids are a critical class of medications that treat both chronic and acute pain that is a serious and costly public health issue [1-4]. The prototypical opioid analgesic, Morphine (**Fig. 1**), is on the World Health Organization (WHO) model list of essential medicines, the most important medications needed in a basic health system. However, its effective analgesic efficacy is accompanied by a series of adverse side effects [5], such as respiratory depression, constipation, nausea and addiction. Therefore, it is an urgent and significant task to develop novel effective analgesics without these deleterious side effects.

Opioid drugs are classified according to three major classes of opioid receptors: mu (μ), delta (δ) and kappa (κ)[6], which are members of class A (rhodopsin-like) G protein coupled receptor (GPCR) family, the largest and most diverse group of membrane receptors and the targets for a large portion of currently used medications[6-8]. The analgesic effect of Morphine is achieved via a classical heterotrimeric G_i protein pathway, which is mediated by the activated mu-opioid receptor (MOR) (**Fig. S1**), leading to the hyperpolarization of neurons and suppression of neuronal excitability [9]. By contrast, most unwanted Morphine-induced side effects associated with tolerance, respiratory depression and constipation are likely attributed to β-arrestin pathway[10-13]. Recently, substantial attention has been focused on development of MOR biased agonists that can specifically trigger G protein signaling pathway over β-arrestin pathway, in order to achieve the goal of providing effective analgesics with reduced side effects. Therefore, understanding the G protein biased mechanism of MOR is important for this class of drug design and development.

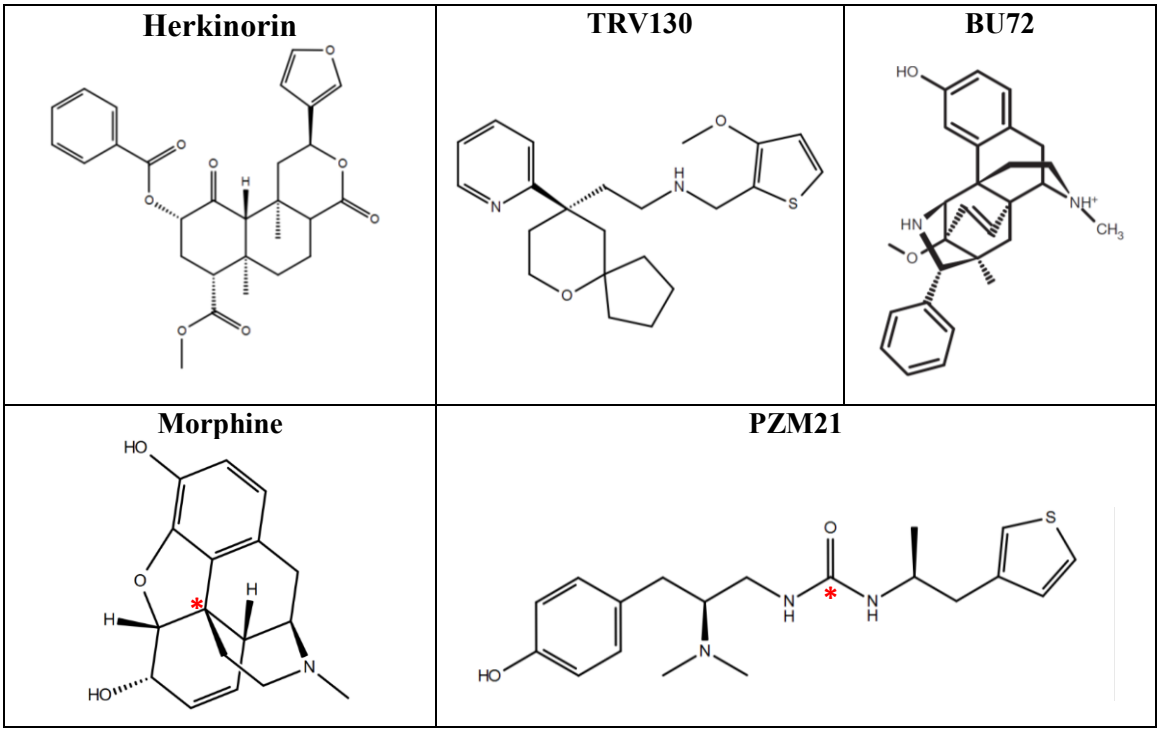

Fig 1. 2D structures of four MOR agonists, Herkinorin, TRV130, BU72, PZM21 and Morphine. The red asterisks of morphine and PZM21 indicate the carbon atoms defined as the nodes to represent the ligands for communication network analysis.

Several G protein biased agonists of MOR have been discovered. Herkinorin (**Fig. 1**) was the first G-protein biased agonist that does not promote the β-arrestin-2 recruitment and does not induce receptor internalization [14]. TRV130 (**Fig. 1**) was another G-protein biased agonist with robust G protein signaling and less β-arrestin recruitment[15], exhibited promising analgesic effect in clinical trials[16], although it finally was not approved by the Food and Drug Administration (FDA) of USA due to concerns that its benefit did not exceed its risk. The latest G-protein biased agonist, PZM21 (**Fig. 1**), showed effective analgesic results and minimal respiratory depression and reinforcing activity in mice, was developed in 2016 through structure-based discovery and high throughput screening[17]. The study showed that PZM21 preferentially activated the G_i protein pathway over β-arrestin-2 pathway, and its G protein bias was similar to TRV130 but over

Herkinorin[17]. Of note, PZM21 showed an unprecedented selectivity for activating MOR, whereas TRV130 was also able to activate the kappa-opioid receptor (KOR) as potent as Morphine[17]. Additionally, PZM21 and TRV130 appeared to interact MOR with distinct binding poses in the MOR orthosteric binding site by docking and molecular dynamics (MD) simulation studies, likely contributing to PZM21's unique selectivity for the MOR compared to TRV-130, although they had similar levels of biased signaling or functional selectivity[17].

GPCR induces G protein or β-arrestin recruitment after activation by an agonist binding, which is an allosteric process transducing signals from the extracellular ligand-binding region to the distant cytoplasmic G protein- or arrestin-binding region. Molecular dynamics (MD) simulation is a powerful tool to investigate the conformational dynamics of a bimolecular system to understand its function and interaction mechanism [18-23]. Recently, MOR's activation mechanism induced by TRV130 was studied widely by MD simulations and experiments. Schneider *et al*. investigated the binding of TRV130 to the activated crystal structure of MOR (PDB: 5C1M) by MD simulations and suggested some important residues contributing to allosteric signal transmission for Morphine and TRV130[24]. Cheng *et al*. performed a series of MD simulations and found that TRV130 stabilized $W^{6.48}$ by interacting with $Y^{7.43}$ through a hydrophobic ring (Superscript numbers refer to Ballesteros-Weinstein residue numbering method for GPCRs[25]), which was important for TRV130 to activate the G protein-biased pathway of MOR[26]. Moreover, Okude *et al*. used NMR spectroscopy to clarify the conformational equilibrium of MOR in the sates bound to different ligands [27]. MOR existed in equilibrium between the closed and open conformations in Morphine-bound state, and in TRV130-bound state, MOR was also in equilibrium between the closed and open conformations, but the open conformation was transformed into a conformation with a larger intracellular cavity[27]. Although these studies provided valuable information about

the G protein biased mechanism of MOR, the dynamic propagation of MOR G protein biased signaling remain unclear, particularly in PZM21-bound state. Therefore, it is necessary to understand how PZM21 activates human MOR to clarify the preferred PZM21-bound MOR conformation for design of new improved analgesics.

In the study, homology modeling, docking and MD simulations were carried out to understand the functional selectivity mechanism of the G protein biased agonist PZM21 for further development of G-protein biased agonists as new analgesics. Using all atom MD simulations, the differences between Morphine and PZM21 in docking poses, residue interactions, conformational changes, molecular switches and dynamic networks were analyzed to understand PZM21's action mechanisms with human MOR.

2. Materials and Methods

2.1. Homology modeling

The pre-aligned crystallographic structure of the active, mouse MOR-1 (the primary MOR variant) bound to the agonist BU72 (**Fig. 1**) in membrane was downloaded from the OPM web server [28] (PDB ID: 5C1M). Firstly, the co-crystal molecule Nanobody39 was deleted, and the complex MOR-BU72 was prepared, optimized and minimized with an OPLS3 force field[29] by using the protein preparation wizard[30] implemented in Maestro 10.3[31, 32]. The FASTA sequence (P35372) of human MOR-1 was taken from UniProt[33], and then human MOR homology model was built with above prepared mouse MOR-1 structure as a template by using the Prime module of Maestro 10.3. Finally, the human MOR-1 homology structure was further optimized and minimized in protein preparation wizard[30].

2.2. Ligand preparation

Two dimensional (2D) structures of Morphine and PZM21 were built in 2D sketcher of Maestro, and they were converted into 3D structures. The ionization/tautomeric states of the three ligands, original crystal ligand BU72, Morphine and PZM21, were generated at pH=7 using Epik (an empirical pKa prediction program) calculation [30]. Finally, each ligand was optimized by minimizing the potential energy to relax with default parameters.

2.3. Ligand docking

The two receptor grid files were generated respectively from the two prepared receptors, mouse MOR-1 (PDB ID: 5C1M) and human MOR-1 homology structure, using Receptor Grid Generation program. The original crystal ligand BU72 was selected to specify the active site and the grid box was generated around it with a Van der Waals radius scaling factor of 1.0 and a partial charge cutoff of 0.25. Then, BU72 was docked to the mouse MOR-1 to validate the docking methodology.

Next, Morphine and PZM21 were respectively docked to the human MOR-1 homology structure using Glide extra precision (XP) docking function with default parameters [34, 35]. The glide-XP-docking procedure performed a systematic search for the best ligand orientation to simulate the most frequently occupied binding pose. Finally, the two Glide XP docking models without crystal waters were respectively submitted to the 2 runs of ~3.5 μs MD simulations.

Additionally, the crystal waters in binding site are important, since some of them are involved in key interactions with the crystallographic ligand BU72 [36], and the induced fit docking can more accurately predict ligand binding modes [37], accompanying by the structural changes in the receptor, than the Glide XP docking does. In order to consider the effect of the crystal waters on the interactions as well as the conformational changes of receptor, the induced fit docking

calculations were further performed using XP sore function and trimming of side chains, after the Glide XP docking calculations were performed in the presence of the crystal waters within 5Å of crystal ligand BU27. The top binding pose with the lowest XP score was selected as the preferred induced fit docked pose for each system. Finally, the two preferred induced fit complexes with the crystal waters were also respectively submitted to the 2 runs of ~1.0 μs MD simulations.

2.4. Simulation system setup

MD simulations were run for above docked complexes, human MOR-1 homology structure in complex with Morphine and PZM21, using the Molecular Dynamics program [38, 39] of Maestro 10.3. Each complex was placed in a biologically relevant membrane of phosphatidylcholines (POPC) lipids[40] and solvated in an orthorhombic water box with a buffer distance of 10Å using simple point-charge (SPC) water model[41]. Then, the system was neutralized using Na^+ ions and was added with a salt concentration of 0.15 M NaCl. Lastly, an optimized potential for liquid simulations 3 (OPLS3) force field[29] was used to model the receptor-ligand-lipid complex.

2.5. MD Simulation

Using Desmond module, each system was relaxed using default relaxation protocols for membrane proteins[42]. In order to avoid possible steric stress, the relaxation protocols were performed and included the following stages: (1) the system was minimized with restraints on solute heavy atoms and then without any restraints; (2) the system was gradually heated from 0 K to 300 K with H_2O barrier and gradual restraining; (3) the system was simulated under the NPT ensemble (constant number of particles, P=1 bar and T=300 K) with H_2O barrier and with heavy atoms restrained; (4) the system was simulated under the NPT ensemble with equilibration of solvent and lipids, then with protein heavy atoms annealing from 10.0 kcal/mol to 2.0 kcal/mol, then with C_α atoms restrained at 2 kcal/mol, and lastly for 1.5 ns with no restraints. After the

relaxation, two independent ~3.5 μs (and ~1.0 μs for the systems with the crystal waters) production runs for the systems without the crystal waters were conducted under the NPT ensemble (P=1 bar and T=310 K) for each of the two systems using the default protocol. During the simulation, the M-SHAKE algorithm[43] was used to constrain all covalent bonds including hydrogen atoms with a 2.0 fs time step, the k-space Gaussian split Ewald method[44] was used to handle long-range electrostatic interactions under a periodic boundary condition with charge grid spacing of ~1 Å and the direct sum tolerance of 10^{-9}, and the Van der Waals interactions were obeyed a uniform density approximation with a non-bonded cutoff of 9 Å. To reduce overload of the computation, non-bonded forces were calculated using an r-RESPA[45] integrator in which the short range forces were updated every step and the long range forces were updated every three steps. For each ligand, the trajectories were saved at 50.0 ps intervals.

2.6. Simulation interaction diagram (SID) analysis

Desmond SID tool was used to analyze the behavior and interaction of protein and ligand during the course of a simulation. The data obtained from the simulation included: root mean square deviation (RMSD), ligand-protein contacts (hydrogen bond, hydrophobic, ionic and water-bridge contacts), protein Secondary Structure Element (SSE), and Root Mean Square Fluctuation (RMSF).

2.7. Trajectory Clustering Analysis

Desmond trajectory clustering tool [46] was used to group complex structures from the combined trajectories of each system. A backbone RMSD matrix was used as a structural dissimilarity metric, and the hierarchical clustering with average linkage was selected as the clustering method with the merging distance cutoff set to 2.5 Å. The centroid structure in the most abundant clusters was used to represent the structural family.

2.8. MOR conserved residues analysis

It is well known that conserved residues are very important in maintaining the function of a protein. In order to find the conserved residues of MOR, one sequence alignment between human MOR and **64** members in class A GPCR family PFAM (seed) PF00001 database[47], and another between human MOR and **11** members in class A GPCR subfamily A4 database, were performed by Mafft web service in Jalview program[48].

2.9. Dynamical Network Model

The MD simulation trajectories of each system were used to generate a dynamic network represented by a set of nodes with connecting edges[49-52], using the NetworkView plugin[53] in VMD[54]. In dynamical networks, protein residues and small molecule substrates are represented by nodes, and previous studies [49-52] showed the nodes located at specific atoms, C_α for protein residue and the center of mass for small molecule, were appropriate. In this study, the C_α atoms of MOR were defined as the nodes to represent the residues of the receptor, and the mass center atoms (**Fig. 1**) of Morphine and PZM21, were defined as the nodes to respectively represent the two ligands. For each system, a contact map was generated by adding edges between nodes if the heavy atoms of two nodes are within 4.5 Å for at least 75% of the MD simulation. The distance d_{ij} or weight w_{ij} of an edge between two nodes (i and j are nodes) is the probability of information transfer across the edge and is calculated from the correlation value (C_{ij}) using the program Carma[55] with the following calculation: $d_{ij} = w_{ij} = -\log(|C_{ij}|)$[51], where, $C_{ij} = \frac{\langle \Delta\vec{r_i}(t) \cdot \Delta\vec{r_j}(t) \rangle}{(\langle \Delta\vec{r_i}(t)^2 \rangle \langle \Delta\vec{r_j}(t)^2 \rangle)^{1/2}}$ and $\Delta\vec{r_i}(t) = \vec{r_i}(t) - \langle\vec{r_i}(t)\rangle$. The thickness of each edge is scaled by distance or weight, and thicker edges show greater correlation[50].

The original Network was then further grouped into different sub-networks called communities, where nodes had more and stronger connections within their community than to nodes in other

communities[52], by using the Girvan-Newman algorithm[56]. Among the nodes in the interface between pairs of communities, the ones that transfer a relatively large degree of information across their edge are called critical nodes[51]. Since critical node pairs carry out intercommunity cross talk, they might be important sites for allosteric signaling transmission.

Finally, optimal and suboptimal paths from ligand (or key residue) to molecular switch residue (or the intracellular end residue of TM) were generated with edge distances offset of 20 Å, in order to identify how the allosteric signals transmit from ligand to intracellular region. A path between two nodes is a set of nodes and connecting edges, and the path length is the sum of distances for all edges in the path[51]. The shortest path is called optimal path and other slightly longer paths are called suboptimal paths[52].

2.10. Normal Mode Analysis

Normal mode analysis (NMA) [57] is a powerful computational method to investigate the vibrational motion of a protein modeled as a harmonic oscillating system that can undergo around a stable equilibrium. The trajectories of Morphine and PZM21 systems were submitted to the VMD Normal Mode Wizard [58] to generate top five motion modes by using the principal component analysis (PCA) [59], a covariance-matrix-based mathematical technique for reducing the dimensionality of large datasets of variables.

3. Results

3.1. The homology model of human MOR-1 is credible, and the dockings revealed similar main interactions of Morphine and PZM21 with the two residues D149$^{3.32}$and Y150$^{3.33}$.

Since no high resolution structure of human MOR is present, and sequence alignment between

human MOR-1 and mouse MOR-1(5C1M) share 97.6% similarity (**Fig. S2**), we built a homology structure of human MOR-1 based on the crystallographic structure of mouse MOR-1 (5C1M)[60], and the two structures were superimposed very well (**Fig. S3**). Furthermore, when viewing the Ramachandran plots of the homology human MOR-1 before and after minimization (**Fig. S4**), it shows that the majority of the black points that represent amino acids are located within the red regions indicating sterically favored regions for alpha-helix and beta-sheet conformations indicating that there are no steric clashes. While there are a smaller group of black points that are located in the yellow regions showing sterically allowed regions. Whereas, only one black dot and two black dots are located in white regions which indicates that they are in the sterically disallowed regions before and after minimization using the default parameters, respectively. Additionally, the total energy of homology human MOR-1 decreased by 916.36 kcal/mol after minimization. Therefore, the built homology structure of human MOR-1 is credible.

The Glide XP docking method was validated by docking crystal ligand BU72 back to its protein crystal-structure, mouse MOR-1 (PDB: 5C1M). The superimposition of the original crystal ligand pose and the newly docked pose shows an excellent overlap with the RMSD value of 0.22 Å, thus validating the feasibility of the XP docking method (**Fig. S5**). Morphine and PZM21 were then docked to the human MOR-1 homology structure with the same parameters, producing the most frequently occupied binding pose of each ligand in the receptor. Both Morphine and PZM21 adopted the orthosteric binding site of human MOR-1 and primarily made similar ionic, hydrogen-bonding and hydrophobic interactions with $D149^{3.32}$ and $Y150^{3.33}$, respectively (**Fig. S6**). Overlap of the original crystal complex (5C1M) with the morphine-docked complex reveals a slight dissimilarity in orientation of its multi-ring structure to BU72's (**Fig. S7A**); overlap of the crystal complex with PZM21-docked complex shows reasonable overlap, perhaps facilitated by PZM21's

rotatable structure (**Fig. S7B**). However, a limitation of Glide XP docking is that the receptor protein was treated as a rigid structure without binding-induced conformational change. In reality, the receptor is more dynamic and will change conformation to accommodate different ligands. To address this limit, two independent ~3.5 μs MD simulations for each of the two docking complexes were further carried out to provide more accurate binding poses and conformational changes.

3.2. The RMSD values showed larger conformation change for PZM21-receptor complex than the Morphine-receptor complex.

To check convergence of the MD simulations, the RMSD values, averaged over the two independent ~3.5 μs MD simulations of receptor protein carbons (C_α) and ligand for Morphine and PZM21 systems were calculated (**Fig. 2**). Relatively flat plots were observed after 1500 ns, indicating the two complex systems have reached new steady states. In Morphine system, protein RMSD stabilized at 1000 ns and remained stable throughout the simulation at ~3.5 Å; and ligand RMSD is stable during the first 2500 ns at ~1.2 Å, and then slightly increases to ~1.5 Å during the last 1000 ns MD simulation. In PZM21 system, protein RMSD reached a stable state at ~3.8 Å after 800 ns, although it had some fluctuations throughout the remaining simulation; ligand RMSD reached a stable state at ~3.5 Å after 1300 ns. Obviously, the ligand RMSD values of PZM21 system are larger than that of Morphine system, indicating the conformational change of PZM21 is larger than that of Morphine. In addition, the RMSD plots of the two systems in each MD simulation (trajectories **1** and **2**) also show relatively flat during the last 500ns (**Figs. S8-S9**), although PZM21 system has some bigger fluctuations.

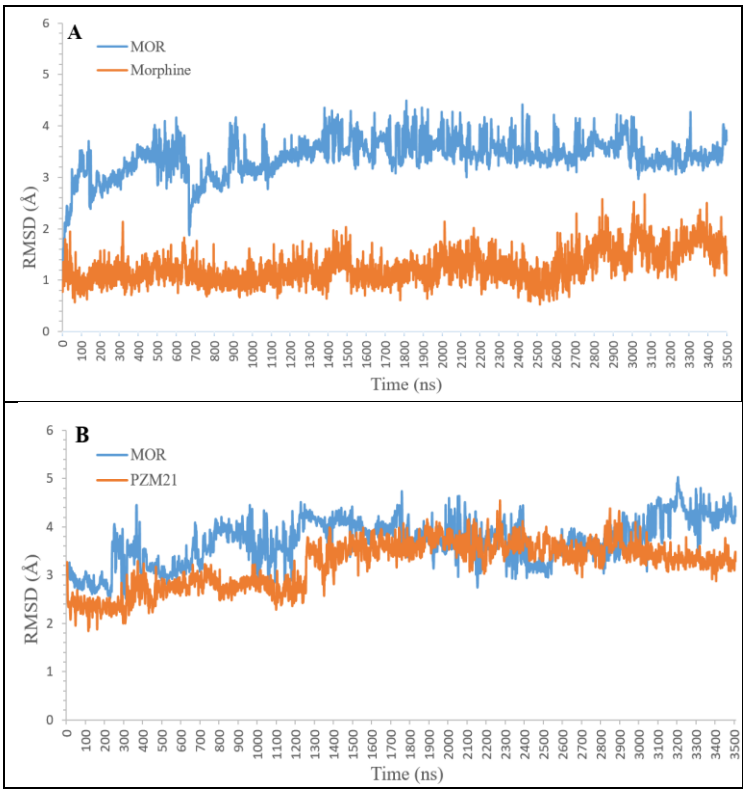

Fig. 2. RMSD values averaged over two independent ~3.5 μs MD simulations of receptor MOR C_α (blue) and ligands (orange) for the Morphine-MOR (**A**) and PZM21-MOR (**B**) complexes are shown.

3.3. Ligand-receptor interaction data show that PZM21 interacts strongly with Y328$^{7.43}$ of TM7, besides the residues (Asp149$^{3.32}$ and Tyr150$^{3.33}$) of TM3.

The ligand-protein interactions for Morphine and PZM21 complexes during each ~3.5 μs MD simulation were calculated using the SID tool. Specifically, the ligand-protein interactions lasting more than 20% of each MD simulation are shown in the 2D interaction diagrams as **Fig. 3**. In trajectories **1** and **2**, the interaction modes of Morphine in binding site were almost the same, except for the hydrogen-bonding interaction with D56$^{N\text{-term}}$ in trajectory **1**. In contrast, although PZM21 maintained these key ionic, hydrogen-bonding and hydrophobic interactions with D149$^{3.32}$ and Y150$^{3.33}$ in the two trajectories as Morphine, its interaction modes were subtly different, i.e., the

hydrogen-bond interaction with Y328$^{7.43}$ enhanced greatly in in trajectories **2**. Moreover, the interaction histograms along with the fraction of each MD simulation for each type of interaction are also shown in **Fig.4**. Clearly, Morphine and PZM21 have similar interactions with D149$^{3.32}$ and Y150$^{3.33}$. Most opioid ligands with different scaffolds were found to be able to form a canonical ionic interaction or H-bond with D149$^{3.32}$ of opioid receptors [36, 61, 62]. As anticipated, both Morphine and PZM21 in both trajectories **1** and **2** did form ionic and hydrogen-bonding interactions with D149$^{3.32}$, with interaction fractions more than 100% for Morphine and more than 85% for PZM21 (**Fig.4**). It is known that the active state of agonist-activated GPCR without bound to its transducer G protein or arrestin is probably unstable, which is reflected in the agonist's lower binding affinity, such as MOR, with its affinity to agonist BU72 decreased by 47-fold when not coupled to the G_i protein[36]. In the case, the interactions of Morphine and PZM21 with D149$^{3.32}$ might be dynamic during the simulations due to their typical binding poses of morphinan-derivatives was not stable enough when without the transducer. Therefore, the ionic interaction fraction of Morphine with D149$^{3.32}$ being only showed ~45% in our simulations is reasonable, further indicating that our MD simulation models for the two systems were reliable. Simultaneously, both Morphine and PZM21 in both trajectories **1** and **2** form hydrophobic interactions with Y150$^{3.33}$, with interaction fractions more than 75% for Morphine and more than 60% for PZM21. Specially, PZM21 can strongly form hydrophobic and H-bonding interactions with Y328$^{7.43}$, with interaction fractions more than 40% in trajectory **1** and more than 100% in trajectory **2**, respectively. The subtle difference in interaction modes between Morphine and PZM21 systems might be related to their signal pathways.

Of note, the two independent simulations (trajectories **1** and **2**) can't completely reproduce the same results, although the key ionic, H-bonding and hydrophobic interactions with D149$^{3.32}$ and

Y150$^{3.33}$ were maintained during MD simulations. It may be because that the active state of agonist-MOR complex in absence of the transducer wasn't stable enough as its inactive state[36], and MD simulation time (several microseconds) is far less than real experimental interaction time (a few minutes) due to calculation limitations.

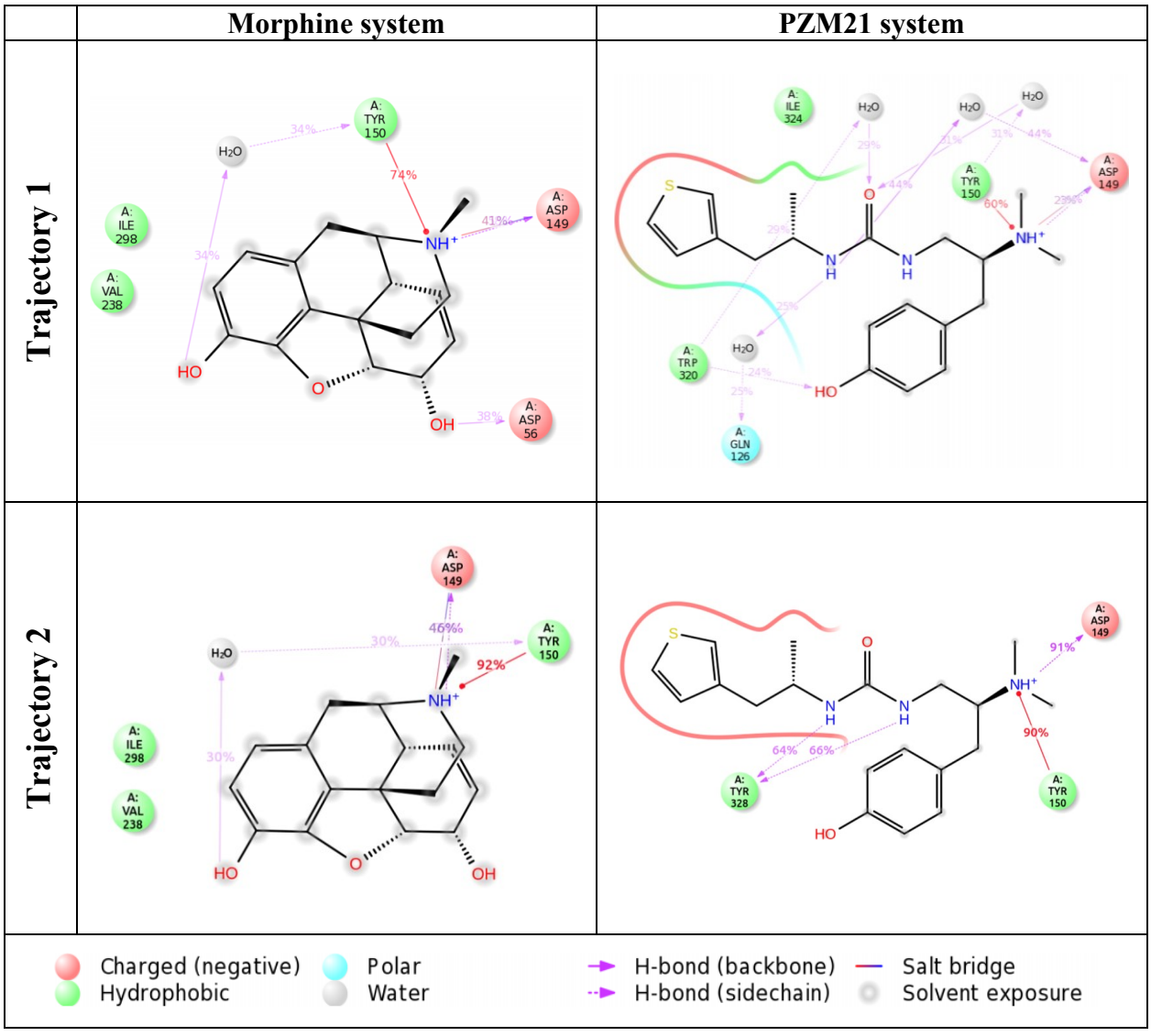

Fig. 3. 2D Interaction Diagrams of Morphine and PZM21 systems during the two independent ~3.5μs MD simulations (Trajectory **1** and Trajectory **2**). The Protein-Ligand interactions lasting more than 20% of the each MD simulation are shown.

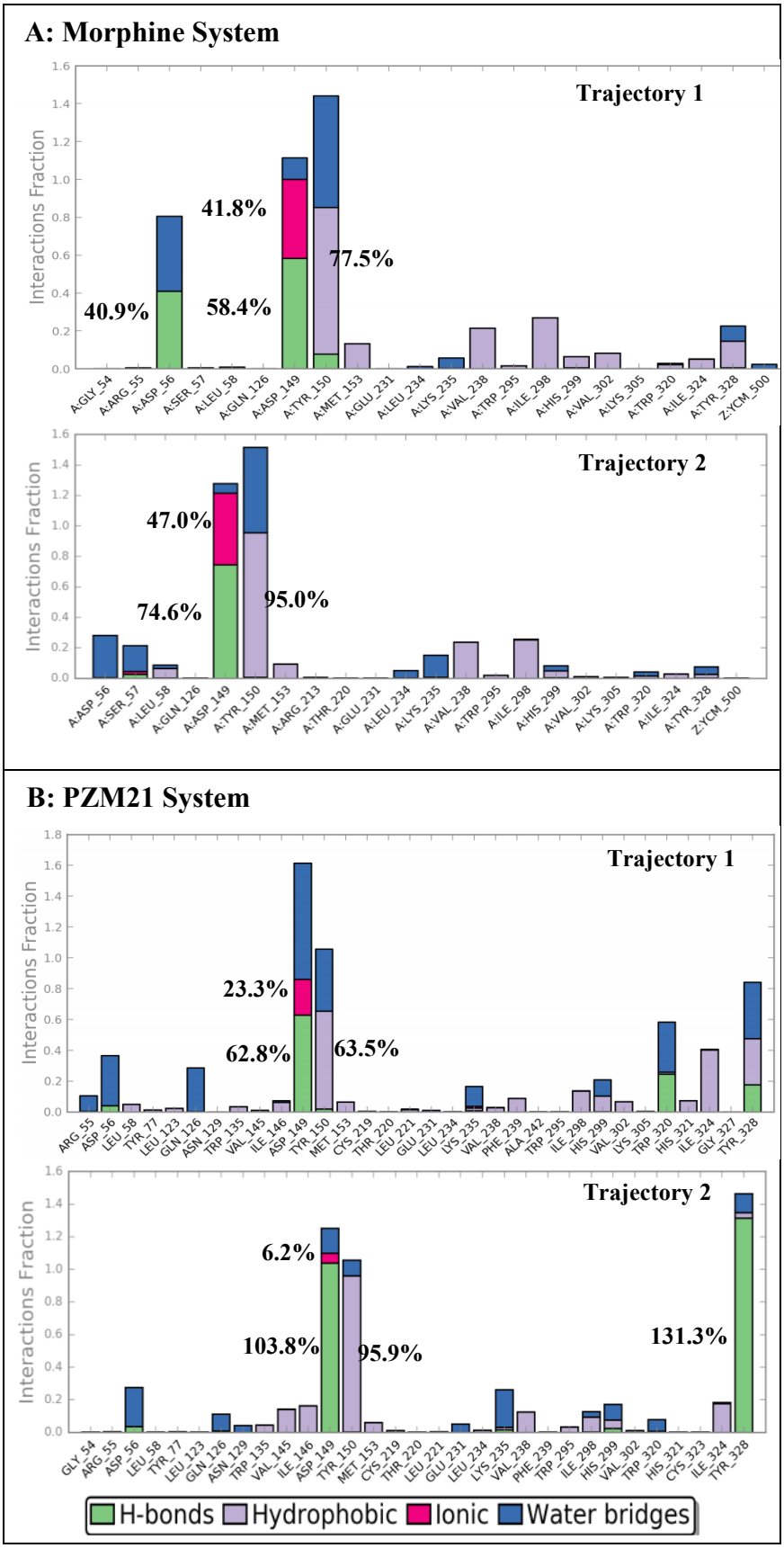
A: Morphine System
Trajectory 1
Interactions Fraction
40.9%
41.8%
58.4%
77.5%
A:GLY_54
A:ARG_55
A:ASP_56
A:SER_57
A:LEU_58
A:GLN_126
A:ASP_149
A:TYR_150
A:MET_153
A:GLU_231
A:LEU_234
A:LYS_235
A:VAL_238
A:TRP_295
A:ILE_298
A:HIS_299
A:VAL_302
A:LYS_305
A:TRP_320
A:ILE_324
A:TYR_328
Z:YCM_500
Trajectory 2
Interactions Fraction
47.0%
74.6%
95.0%
A:ASP_56
A:SER_57
A:LEU_58
A:GLN_126
A:ASP_149
A:TYR_150
A:MET_153
A:ARG_213
A:THR_220
A:GLU_231
A:LEU_234
A:LYS_235
A:VAL_238
A:TRP_295
A:ILE_298
A:HIS_299
A:VAL_302
A:LYS_305
A:TRP_320
A:ILE_324
A:TYR_328
Z:YCM_500
B: PZM21 System
Trajectory 1
Interactions Fraction
23.3%
62.8%
63.5%
ARG_55
ASP_56
LEU_58
TYR_77
LEU_123
GLN_126
ASN_129
TRP_135
VAL_145
ILE_146
ASP_149
TYR_150
MET_153
CYS_219
THR_220
LEU_221
GLU_231
LEU_234
LYS_235
VAL_238
PHE_239
ALA_242
TRP_295
ILE_298
HIS_299
VAL_302
LYS_305
TRP_320
HIS_321
ILE_324
GLY_327
TYR_328
Trajectory 2
Interactions Fraction
6.2%
103.8%
95.9%
131.3%
GLY_54
ARG_55
ASP_56
LEU_58
TYR_77
LEU_123
GLN_126
ASN_129
TRP_135
VAL_145
ILE_146
ASP_149
TYR_150
MET_153
CYS_219
THR_220
LEU_221
GLU_231
LEU_234
LYS_235
VAL_238
PHE_239
TRP_295
ILE_298
HIS_299
VAL_302
TRP_320
HIS_321
CYS_323
ILE_324
TYR_328
H-bonds
Hydrophobic
Ionic
Water bridges

Fig. 4. Protein-Ligand interactions (**A**: Morphine system; **B**: PZM21 system) of the two independent ~3.5 μs MD simulations (Trajectory 1 and Trajectory 2). All residues that interact with the ligand are shown in the histogram along with the interactions fraction for each type of interaction and some fraction values of key residues are labelled.

3.4. Clustering analysis showed the PZM21's receptor exhibited more diversified conformations and formed a larger intracellular cavity due to the stronger outward bending on the intracellular ends of TM5-7.

To identify major binding poses for each system, we clustered complex structures from the 2 runs of ~3.5 μs MD simulations and aligned them. The representative structures in top abundant clusters (>5.0%) are shown in **Fig. S10**. Morphine's dominant cluster has an abundance of 91.1%, with only one other cluster (8.1%); but PZM21 adopts numerous clusters, with its most abundant cluster at 35.5%, and following clusters at 21.1%, 8.9%, 8.5% and 7.3%. The result also showed that PZM21 system exhibited bigger fluctuations during MD simulations. Although the ligands Morphine and PZM21 were all bound to the orthosteric binding site of MOR, the PZM21 exhibited more flexible with more diversified conformations than Morphine did. There are existing some complicated reasons to make PZM21 fluctuated more during the MD simulations. These possible reasons are that, the docked pose of PZM21 is different from the real bound state due to limitation of Glide XP docking method or the absence of the crystal waters in the binding sites; the active state of PZM21-MOR complex is probably unstable when without coupling its G protein or arrestin[36]; the structure of PZM21 is more elongated and flexible than Morphine's compact rigid structure; the function and character of PZM21-MOR complex are different from that of Morphine-MOR, and so on. The superimposition of the seven representative structures is shown in **Fig. S11**. In the receptors' extracellular end (top view), some subtle differences are found in the TM1-2 and TM6, along with N-terminal, ECL1 and ECL2. Especially, in the receptors' intracellular end (bottom view), the TM5-7, along with ICL3 and H8, are stretched outward much

stronger in PZM21 system, producing a larger cavity to facilitate the binding of G protein. Moreover, superimposition of each representative structure in the most abundant cluster for Morphine complex (91.1%) and PZM21 complex (35.5%) is shown in **Fig. 5**, which clearly illustrates the subtle differences in ligand-protein contacts. The PZM21 is much elongated with phenol group extending to TM5 and thiophene group extending to the middle between TM2 and TM7. Meanwhile, except for the conformational differences in the extracellular ends of the TM1-2 and TM6, the TM5-7 helices along with ICL3 of the PZM21-bound MOR were also clearly shown a stronger outward bending on the intracellular side. Therefore, the two representative structures in the most abundant clusters can well represent the receptor's conformations, thus they were used for later molecular switch analyses.

In addition, the representative structures of receptor in the most abundant clusters of the two systems as well as the active MOR were also superimposed for comparison (**Fig. S12**). Some differences are also found at the extracellular end of TM1-2 and TM6 of PZM21-bound MOR (top view). Especially, when taking the active MOR as a reference, the intracellular end of TM5-7 and ICL3 of PZM21-bound MOR are stretched outward, but that of Morphine-bound MOR are stretched intward (bottom view). Therefore, The PZM21-bound MOR's intracellular ends of TM5-7 helice were bent outward more strongly even than active MOR.

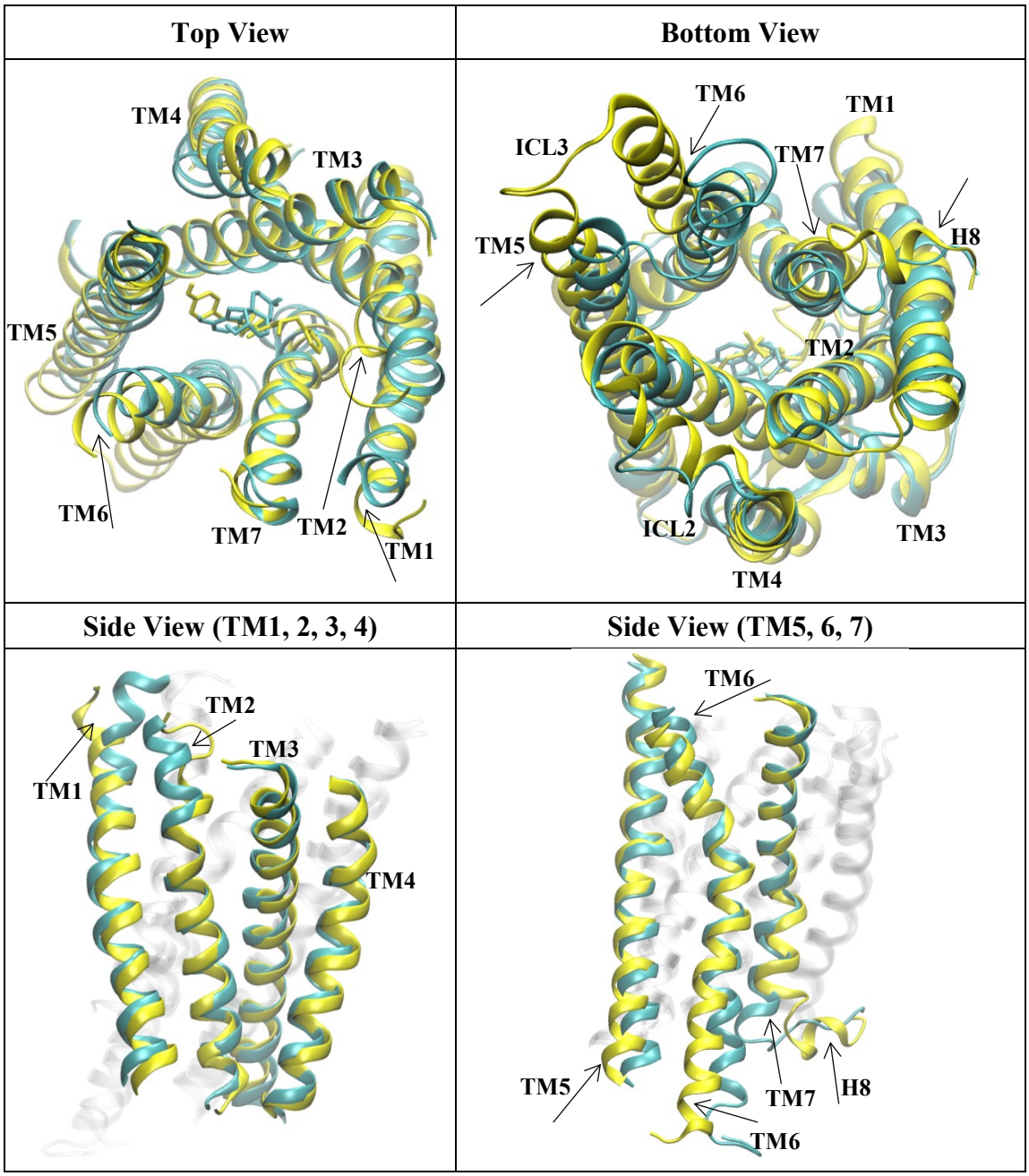

Fig. 5. The representative structures of the most abundant clusters for the Morphine (cyan) and PZM21 (yellow) complexes are superimposed. The receptors are represented by ribbon and the ligands are represented by sticks with the same color as its receptor. For clarity, some intracellular and extracellular loops were omitted and the differences in TMs are marked by arrows.

3.5. The protein Secondary Structure Element (SSE) analyses also identified that the TM5-7 helices of the two systems showed some differences.

In order to investigate differences on the secondary structure of the receptor, the protein SSE analysis in **Fig. 6** for the two systems throughout the two independent ~3.5 μs simulations was also calculated using the SID tool. Noticeable changes in helical structures are observed primarily at TM1-2, TM5-7 and H8. In PZM21 system, the TM1, TM5, ICL2-3 and H8 display greater SSEs indicating increased helical structures of the receptor at these areas, but the TM2 and TM6-7 show smaller SSEs indicating a loss of helical structures with increase of coil structures. These are consistent with the clustering result that PZM21 system's ICL2 and H8 displayed helical structures but its upper part of TM2 displayed a coil as shown in **Fig. 5**. Moreover, these SSE percentage changes of secondary structure must cause relevant changes in corresponding TMs in 3D structure, which could explain why the conformation differences in helices were shown at the TM1-2, TM5-7 and H8 (**Fig. 5**).

It is noted that the role of solvents in the disruption of the SSEs in the two systems was ignored in the study. That is because each of the two complexes was placed in the same solvent environment (POPC lipids, an orthorhombic SPC water box with a buffer distance of 10Å, 0.15 M NaCl salt concentration) in the MD simulations and the same solvent environment would produce the same effect on the two complexes.

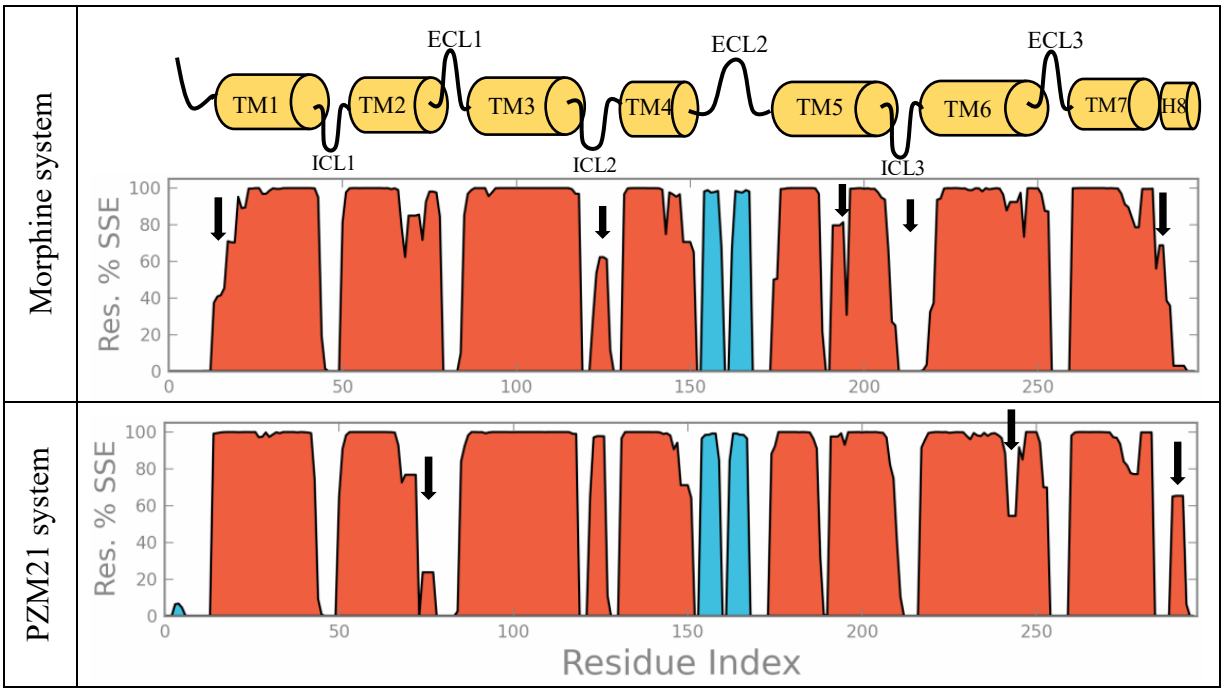

Fig. 6. Protein secondary structure comparison between Morphine system and PZM21 system. Protein Secondary Structure Element (SSE) distributions by residues for each system throughout the two independent ~3.5 μs simulation are shown, where the α-helices are represented in red and the β-strands are represented in blue. Moreover, the differences are marked by black arrows and the above MOR architecture is for reference.

3.6. Protein and ligand RMSF data showed that ligand PZM21 and its receptor's TM5-6 exhibited larger fluctuations compared with Morphine system.

To detect structural fluctuation of protein, the average protein C_α RMSF values were calculated using the SID tool to analyze the fluctuation differences in the two systems during the two independent ~3.5 μs MD simulations (**Fig. 7**). In general, the terminal and loops exhibit higher fluctuation than the TM helices. The greatest RMSF values are exhibited in ICL3, meaning that ICL3 made the greatest fluctuation during the MD simulations. Interesting, the TM5-6 along with ICL3 display greater RMSF values in PZM21 system compare with Morphine system, which may be correlated with their stronger outward bending.

Generally speaking, the RMSF magnitude of the ligand is related to its fluctuation in the binding site. Obviously, the average atom RMSF values of PZM21 are all bigger than that of Morphine (**Fig. 8**). This indicated that PZM21, especially for its phenol group, was more fluctuated in the binding site during the MD simulations, thereby adopting more binding poses as shown as **Fig. S10.**

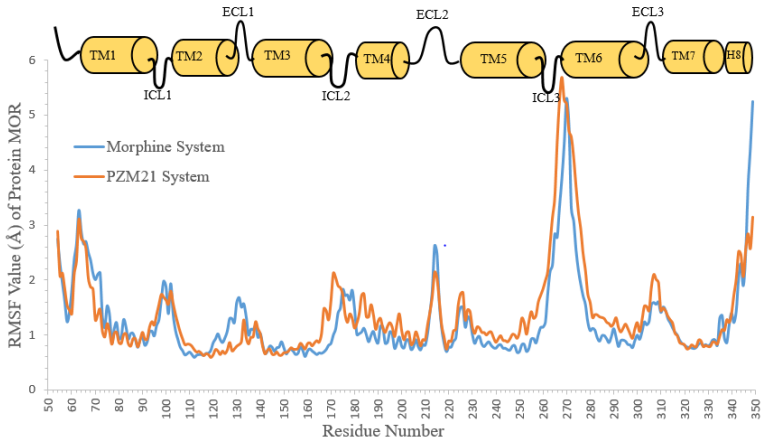

Fig. 7. The protein root mean square fluctuation (RMSF) values, averaged over the two independent ~3.5 μs MD simulations of Morphine system (blue) and PZM21 system (orange). In addition, the above MOR architecture is for reference.

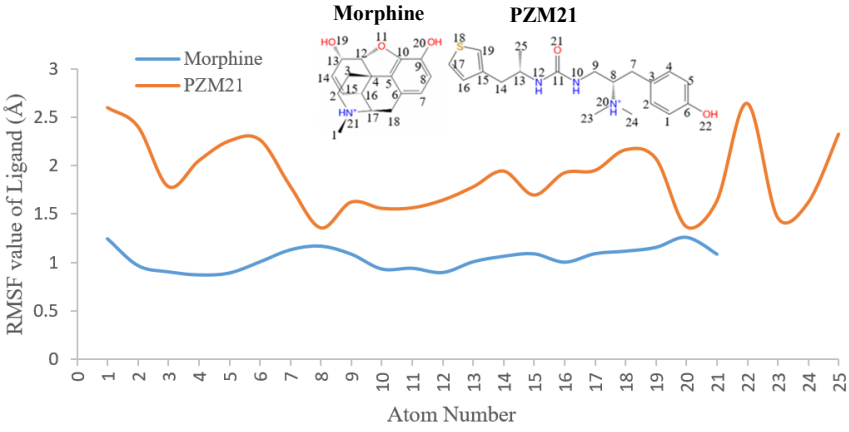

Fig. 8. The ligand atom root mean square fluctuation (RMSF) values, averaged over the two independent ~3.5 μs MD simulations of Morphine (blue) and PZM21 (orange).

3.7. The differences in the ionic lock (DRY), transmission (CWXP) and Tyr toggle (NPXXY) switches between the two systems may be important for PZM21's G protein biased signaling pathway.

Compared with inactive MOR structure (4DKL), the representatively active MOR structures bound with Morphine and PZM21 showed the primary differences on the intracellular ends of TM5-7, with TM5 bending toward TM6, TM6 bending outward, and TM7 bending inward, from the bottom view in **Fig. 9**. This kind of TM movement was appeared on most active GPCR structures[63]. In addition, the TM5-6 helices of the PZM21-bound MOR were bent outward stronger than the Morphine-bound MOR, but its TM7 was bent inward weaker, leading to the larger cavity in the intracellular end of PZM21-bound MOR.

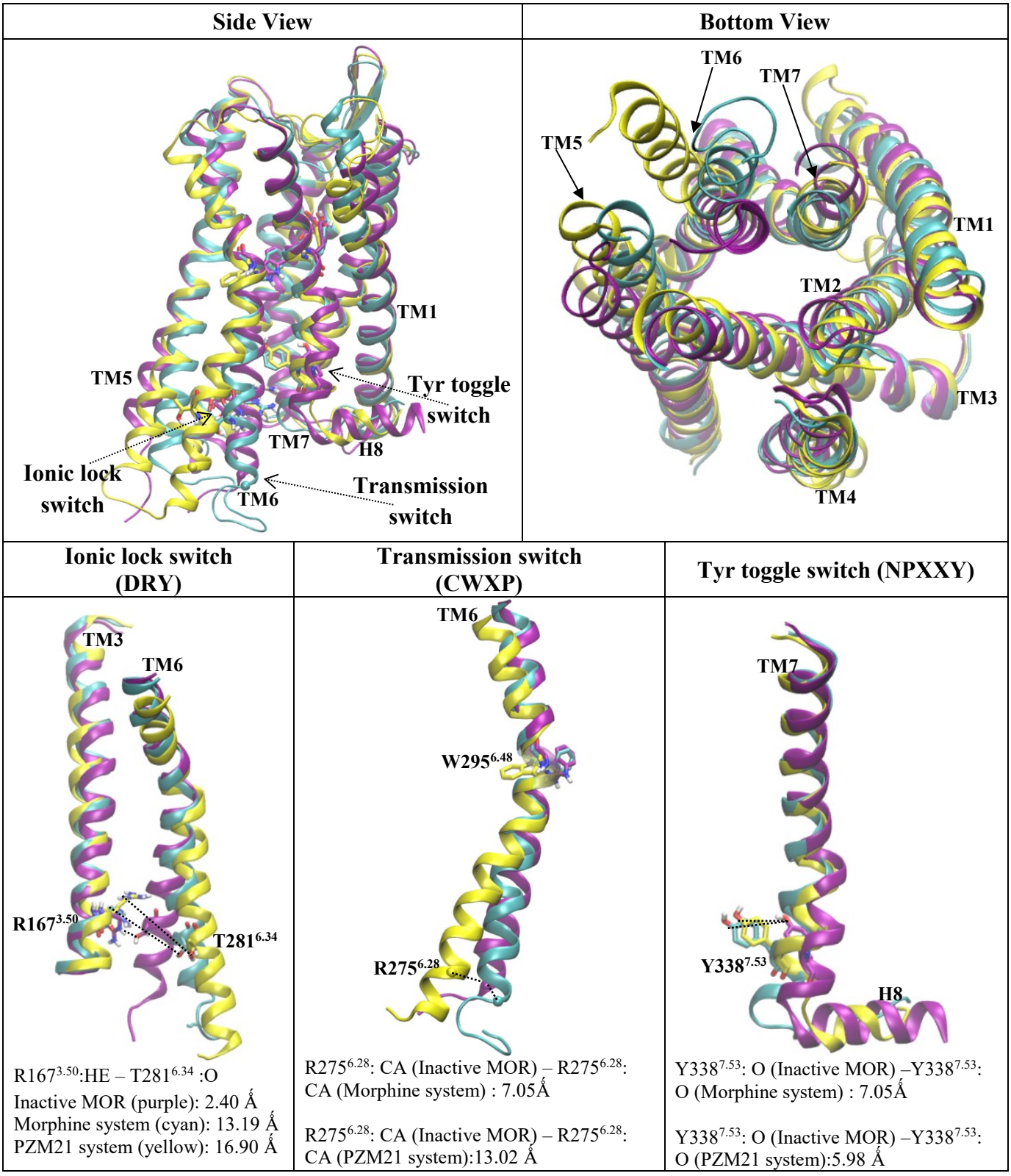

Fig. 9. The Morphine (cyan) and PZM21 (yellow) systems' representative structures of the most abundant clusters obtained from the two independent ~3.5 μs MD simulations, as well as inactive MOR structure (4DKL, purple). These are superimposed for comparison from different views, where molecular switches are compared with each other. Some important distances are marked by

dotted lines and corresponding distance values are also shown.

GPCRs was considered to be able to alternate between the inactive and active states via the conversion of some special molecular switches, and these switches communicate throughout the TM region and play a crucial role in transmitting signals from the extracellular ligand binding site to the cytoplasmic G-protein or arrestin binding site[64]. In **Fig. 9**, the larger differences in the two systems appeared at the the ionic lock (DRY), transmission (CWXP) and Tyr toggle (NPXXY) switches, and PZM21-activated MOR showed stronger outward movement of TM6 intercellular end, stronger rotation of $W295^{6.48}$ to TM5, and weaker inward movement of $Y388^{7.53}$. The transmission switch activation is characterized by the outward movement and rotation of TM6. Along with $W295^{6.48}$ rotating toward TM5, the $R275^{6.28}$ outward movement distance of PZM21-bound MOR (13.02 Å) from the inactive state was almost twice that of Morphine-bound MOR (7.05 Å). The ionic lock switch is a salt bridge formed between $R^{3.50}$ and $E^{6.30}$ in an inactive state, but the acidic residue in position 6.30 is conserved in only about 30% of GPCRs[65]. Instead, the hydrogen bonding interaction between $R^{3.50}$ and $T^{6.34}$ in MOR or KOR may be also important for regulating receptor signaling[65]. The ionic lock switch activation is characterized by its disruption. Accompanied by the stronger outward movement of TM6, the hydrogen bond distance between $R167^{3.50}$ and $T281^{6.34}$ of PZM21-bound MOR (16.90 Å) was longer than that of Morphine-bound MOR (13.19 Å). The Tyr toggle switch activation is characterized by the inward movement of TM7. The $Y338^{7.53}$ distance of PZM21-bound MOR (5.98 Å) from the inactive state was smaller than that of Morphine-bound MOR (7.05 Å), due to the weaker inward movement of TM7. Therefore, the main players important for PZM21's G protein biased signaling pathway may be ionic lock, transmission, and Tyr toggle switches.

Usually, during the activation of GPCR, the outward movement and rotation of TM6 make the distance of ionic-lock residues ($R^{3.50}$ – $E^{6.30}$ or $R^{3.50}$ – $T^{6.34}$) increase and the distance of transmission-switch residues ($W^{6.48}$ – $P^{5.50}$) decrease, and the inward movement of TM7 make the distance of Tyr toggle switch residues ($Y^{7.53}$ – $Y^{5.58}$) decrease[64]. Herein, the distances of the three molecular switches throughout our MD simulations were measured, as shown in **Fig. S13**. In PZM21 system, the distances between ionic-lock residues (i.e., the hydrogen bond distance between $R167^{3.50}$ and $T281^{6.34}$) of trajectory **1** increased to ~19.5 Å at last 500 ns, but that of trajectory **2** fluctuated around 12 Å. It meant that the distance dynamics in the two trajectories of PZM21 system were different at last 500 ns, one increased and one decreased. In contrast, the distance dynamics in the two trajectories of Morphine system were relatively similar. This result showed that the distance of PZM21 system exhibited bigger fluctuations during the MD simulations. Compared the distances averaged over the two trajectories for the two systems, the mean distances during the whole 3.5 μs and the last 500 ns of PZM21 system (14.4 and 15.7 Å) were respectively longer than that of Morphine system (14.2 and 14.7 Å), which potentially agreed with the stronger TM6 outward movement of PZM21 system (**Fig. S11)**. Similarly, the distances between transmission-switch residues (i.e., the geometric center distance of $W295^{6.48}$ and $P246^{5.50}$) of PZM21 system also exhibited bigger fluctuations during the MD simulations than that of Morphine system. During the last 500 ns, the mean distance averaged over the two trajectories of PZM21 system (8.1 Å) are shorter than that of Morphine system (9.1 Å), which might be accompanied by the stronger rotation of $W295^{6.48}$ of PZM21 system. In addition, for the two systems, the distances between Tyr toggle switch residues (i.e., the O atoms distance between $Y338^{7.53}$ and $Y254^{5.58}$) in the two trajectories, all exhibited big fluctuations. While, during the last 500 ns, the distances averaged over the two trajectories of PZM21 system, with mean distance of

6.3 Å, are longer than that of Morphine system, with mean distance of 4.0 Å, which might be correlative with the weaker inward movement of Y338$^{7.53}$ of PZM21 system. Therefore, these distances of molecular switches could reflect well the outward movements of TM5-7 in PZM21 system shown in representative structures (**Fig.9**).

3.8. The MOR conserved residues in class A GPCR and subfamily A4 were obtained by sequence alignments.

The results of the two sequence alignments, one being between human MOR and **64** members in class A GPCR family PFAM (seed) PF00001 database, another being between human MOR and other **11** members in class A GPCR subfamily A4 database, are respectively shown in **Fig. S14** and **Fig. S15**, from which the related percentage identity of MOR residues were obtained and shown in **Table S1**. Subsequently, based on the percentage identity cutoff value of 50%, the MOR conserved residues for class A GPCR and only just for subfamily A4 were respectively selected out in **Table S2** and **Table S3**. Clearly, the residues of ionic lock (DRY), transmission (CWXP) and Tyr toggle (NPXXY) molecular switches are conserved in class A GPCR.

3.9. The distance analyses for 34 residue pairs with conserved change upon activation showed distance increase of some inter-helical residue pairs in PZM21 system.

Recently, Zhou *et al.* discovered a common and conserved class A GPCR activation pathway comprised of 34 residue pairs with conserved rearrangement upon activation[66]. In order to explore the activation pathway difference between Morphine and PZM21 systems, the geometric center distances of the 34 conserved residue pairs during the MD simulations (trajectories **1** and **2**) and related average distances were measured in **Fig. S16**. It is easy to find that most of distances showed similar dynamic trend in the two trajectories, but some distances, especially for V287$^{6.40}$–

N334$^{7.49}$ and Y338$^{7.53}$–F345$^{8.50}$ of Morphine system, V247$^{5.51}$–F291$^{6.44}$ and T251$^{5.55}$–V288$^{6.41}$ of PZM21 system, exhibited larger dynamic difference, thus it is more reasonable to analyze the average distances averaged over the two trajectories. In order to clearly compare the distance changes between the two systems, the average distances during the first 500 ns, last 500 ns and whole 3.5 μs, and related distance changes were further calculated in **Table S4**. For the distance change values between first 500 ns and last 500 ns, all distance changes of Morphine system are smaller, within ±1Å, but some distance change of PZM21 system are larger with more than 1Å or less than -1Å, especially for the distances R167$^{3.50}$–Y338$^{7.53}$ and T251$^{5.55}$–V288$^{6.41}$ with more than 3Å . It means that Morphine system can maintain the distances of the **34** residue pairs in a whole, but PZM21 system can't. The residue pairs of PZM21 system with larger distance change (more than 1Å or less than -1Å) between first 500 ns and last 500 ns were selected out and shown in **Fig. S17**. Obviously, out of these **15** residue pairs, **13** residue pairs increased their distances, which would decrease the contacts between TMs and potentially cause the movements of TMs. To achieve a more reliable conclusion, the average distances during the whole 3.5 μs were further compared between the two systems (**Table S4**). There are five inter-helical residue pairs' distance difference values bigger than 1Å, but only one intra-helical residue pair is smaller than -1Å. It means that the distances of the five residue pairs in PZM21 system increased but one residue pair decreased when compared with Morphine system (**Fig. 10**). Similarly, along with the distance increase of the five inter-helical residue pairs during the whole MD simulations, the PZM21 system would decrease the contacts among TMs and easily cause the outward movements of TMs, potentially leading to the appearance of the larger cavity at the intracellular end of PZM21-bound MOR (**Fig. 9**) and simultaneously affecting its activation pathway.

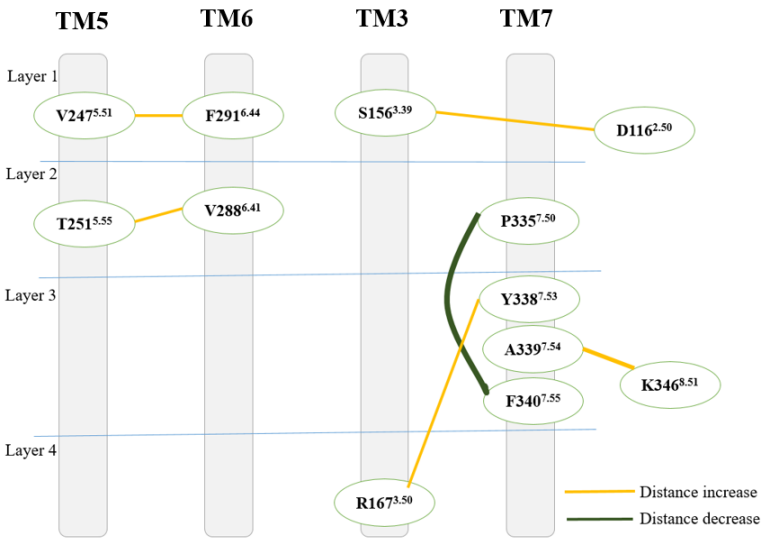

Fig. 10. Compared with Morphine system, the **6** residue pairs of PZM21 system with larger distance difference (more than 1Å or less than -1Å) during the whole ~3.5 μs MD simulations are displayed.

3.10. The distributions of structural communities are clearly different between the Morphine and PZM21 systems, which are closely correlated with the different movements of their TMs.

To decipher allosteric signal transmission pathway, the network models weighted by correlated motion from the two independent ~3.5 μs MD simulations were calculated (**Fig. S18**), where thicker edges indicate higher correlation between two nodes. The weighted network models of the Morphine and PZM21 systems show similar correlations, that is, both top and bottom sections of 7TMs exhibit higher correlations with thicker edges than the middle sections.

The weighted network was then divided into disjoint sub-networks called communities in which nodes connect more frequently and strongly in the same community than to nodes in other community. There are nine communities for the two systems, four associated with the top sections and five associated with the bottom sections (**Fig. 11**). However, the detailed distributions of their

communities are clearly different. The Morphine system shows the bottom sections of TM6 and TM7, and H8 are in the same community (green), whereas the PZM21 system separated them, one (orange) containing the bottom section of TM6 and ICL3, and another (yellow) containing the bottom sections of TM7 and TM1, H8, and the middle section of TM2. It means that the connection between the TM6 and TM7 of PZM21 system is weaker than that of Morphine system, so that the stronger outward bending for the bottom section of TM6 along with ICL3 in PZM21 system was found. Similarly, the Morphine system shows the bottom sections of TM3 and TM5, and ICL2 are in the same community (red), whereas the PZM21 system separated them, one (white) containing the bottom section of TM3 and ICL2, and another (tan) containing the nearly whole TM5. It means the bottom sections of TM3 and TM5 of PZM21system are more flexible, so that the more obviously outward shift of the bottom section of TM5 in PZM21 system was found.

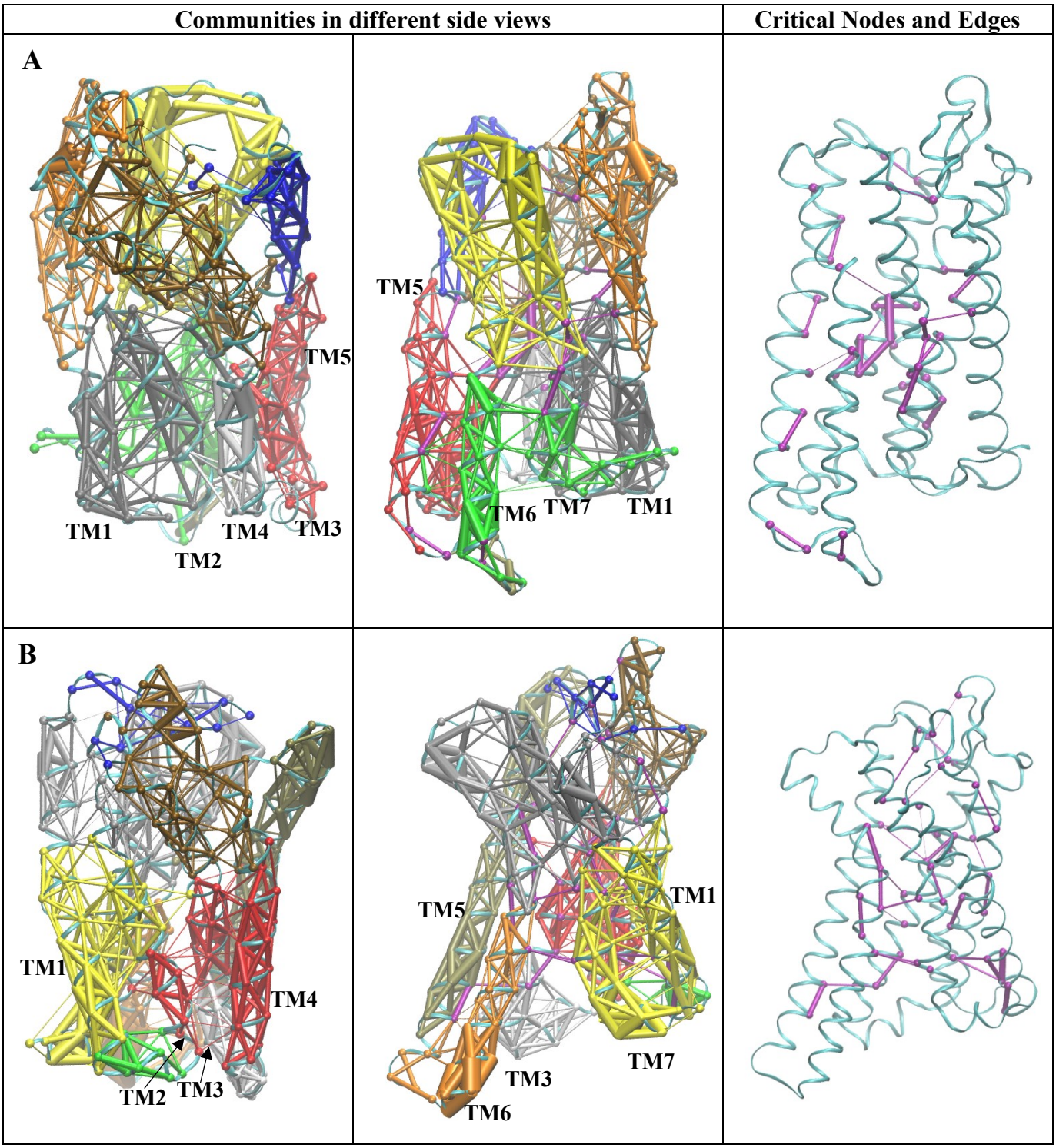

Fig. 11. Structural communities separated by color with the critical nodes and edges in purple are shown for the Morphine (**A**) and PZM21 (**B**) systems. The connection between nodes in the same community is stronger than different communities. Critical nodes represent the strongest signal connection between different communities.

3.11. The critical nodes analyses identified that most critical nodes in the two systems are conserved, which may be very important for their signal transduction.

Critical node pairs are the strongest signal connection between different communities to carry out intercommunity cross talk, so they may play a significant role in signal transduction between different parts of receptor. From above community analysis, there were **43** critical nodes in the Morphine system and **44** in the PZM21 system, where **13** critical nodes are common in both systems (**Table 1**). Since highly conserved residues are critical for activation of GPCRs, these critical nodes were then cross referenced with the literatures [8, 67, 68] and our sequence alignment analyses (**Tables S2-S3**) to identify the key residues that involved in the activation of GPCRs. In **Table 1**, the Morphine system had **31** critical nodes that conserved or were associated with switch motifs, and PZM21 system had **27**.

Table 1. Critical nodes of the Morphine and PZM21 systems from the dynamics network analysis. The residues being in conserved network of non-covalent contacts or highly conserved are displayed in bold, and the residues associated with switch motifs are underlined.

	Morphine system	PZM21 system
Common	D56$^{N\text{-term}}$, L58 $^{N\text{-term}}$, **D116$^{2.50}$**, I148$^{3.31}$, **M153$^{3.36}$**, **I157$^{3.40}$**, **L160$^{3.43}$**, M207$^{4.63}$, **F223^{ECL2}**, **V238$^{5.42}$**, **F291$^{6.44}$**, **S331$^{7.46}$**, **L337$^{7.52}$**	
N-term		P60 $^{N\text{-term}}$
TM1	**V80$^{1.42}$**	**V91$^{1.53}$**, M92$^{1.54}$,**V94$^{1.56}$**, **I95$^{1.57}$**
ICL1		T99 ^{ICL1}
TM2	**I107$^{2.41}$**, **F110$^{2.44}$**, **N111$^{2.45}$**, A119$^{2.53}$, T122$^{2.56}$	**I109$^{2.43}$**, **L112$^{2.46}$**, L114$^{2.48}$, **P124$^{2.58}$**, V128$^{2.62}$, 130$^{2.64}$
TM3	**N152$^{3.35}$**, **F154$^{3.37}$**, **S156$^{3.39}$**, **F158$^{3.41}$**, **C161$^{3.44}$**	**D149$^{3.32}$**, Y150$^{3.33}$, **Y151$^{3.34}$**, **M163$^{3.46}$**, **R167$^{3.50}$**
TM4	**N190$^{4.46}$**, **N193$^{4.49}$**, **L196$^{4.52}$**, **S197$^{4.53}$**	
ECL2		R213^{ECL2}, T220 ^{ECL2}
TM5	N232$^{5.36}$, **L234$^{5.38}$**, **F241$^{5.45}$**, **P246$^{5.50}$**, **I250$^{5.54}$**, **Y254$^{5.58}$**, **I258$^{5.62}$**, **V264$^{5.68}$**	M257$^{5.61}$, **L261$^{5.65}$**
ICL3	**M266^{ICL3}**	
TM6	K273$^{6.26}$, **R275$^{6.28}$**, H299$^{6.52}$, A306$^{6.59}$	**V287$^{6.40}$**, **V288$^{6.41}$**, I292$^{6.45}$, **W295$^{6.48}$**, **I298$^{6.51}$**
TM7	T329$^{7.44}$, **N334$^{7.49}$**	W320$^{7.35}$, H321$^{7.36}$,**Y328$^{7.43}$**, **N330$^{7.45}$**,**Y338$^{7.53}$**

3.12. Optimal and suboptimal paths revealed that the transmission of allosteric signals between the two systems were slightly different.

In order to identify how the allosteric signals transmit from ligand binding pocket to intracellular region, the optimal (the shortest) and suboptimal (slightly longer) paths from the ligand to the residue of each molecular switch (ionic lock switch: $R167^{3.50}$ of TM3; $Y254^{5.58}$ of TM5; transmission switch: $T281^{6.34}$ of TM6; Tyrosine toggle switch: $Y338^{7.53}$ of TM7) were calculated (**Fig. 12**). For the signals to $R167^{3.50}$ of TM3, Morphine's paths pass directly through the TM3, while PZM21's paths primarily pass through TM6. Similarly, for the signals to $Y254^{5.58}$ of TM5, Morphine's paths reach TM5 by crossing TM3, but PZM21's paths need to cross TM7 and TM6. For the signals to $T281^{6.34}$ of TM6, the optimal paths of the two systems are roughly similar by crossing TM7 to get TM6, except for three different residues. For the signals to $Y338^{7.53}$ of TM7, Morphine goes primarily along TM3, TM2 and TM7, whereas PZM21 goes directly along TM7. Therefore, these network paths to the intracellular ends of the three TMs (TM3, TM5 and TM7) are different between the two systems, but the two systems' optimal paths to the transmission switch in the intracellular end of TM6 were similar. On the other hand, some edges in network paths of PZM21 are thinner than that of Morphine (including the edges connecting $W295^{6.48}$ and $I157^{3.40}$, $V288^{6.41}$ and $Y254^{5.58}$, PZM21 and $Y328^{7.43}$), thereby the thinner network signals from PZM21 to the molecular switches of TM3, TM5 and TM7 were a little bit weaker than that from Morphine. In addition, most residues involved in above optimal paths to TM3, TM5, TM6 and TM7 are conserved (**Fig. 12**), supporting that allosteric signaling is evolutionarily conserved for GPCRs [69].

Since previous study showed that the conformation of TM6 is related to the efficiency of G protein coupling and the conformation of TM7 is related to the efficiency of arrestin coupling[70],

we further calculated the network paths from the key contact residues D149$^{3.32}$ and Y150$^{3.33}$ to the end of TM6 (S270$^{6.23}$) and TM7 (L341$^{7.56}$) (**Fig. S19**). For the two systems, the paths from D149$^{3.32}$ or Y150$^{3.33}$ to the end of TM6 (S270$^{6.23}$) are roughly similar with most network nodes locating at TM3 and TM6, while the paths to the end of TM7 (L341$^{7.56}$) are different with most network nodes for Morphine system locating at TM3 but for PZM21 system locating at TM7. These different network paths to the intracellular end of MOR might cause the differences in allosteric signal transmission between the two systems.

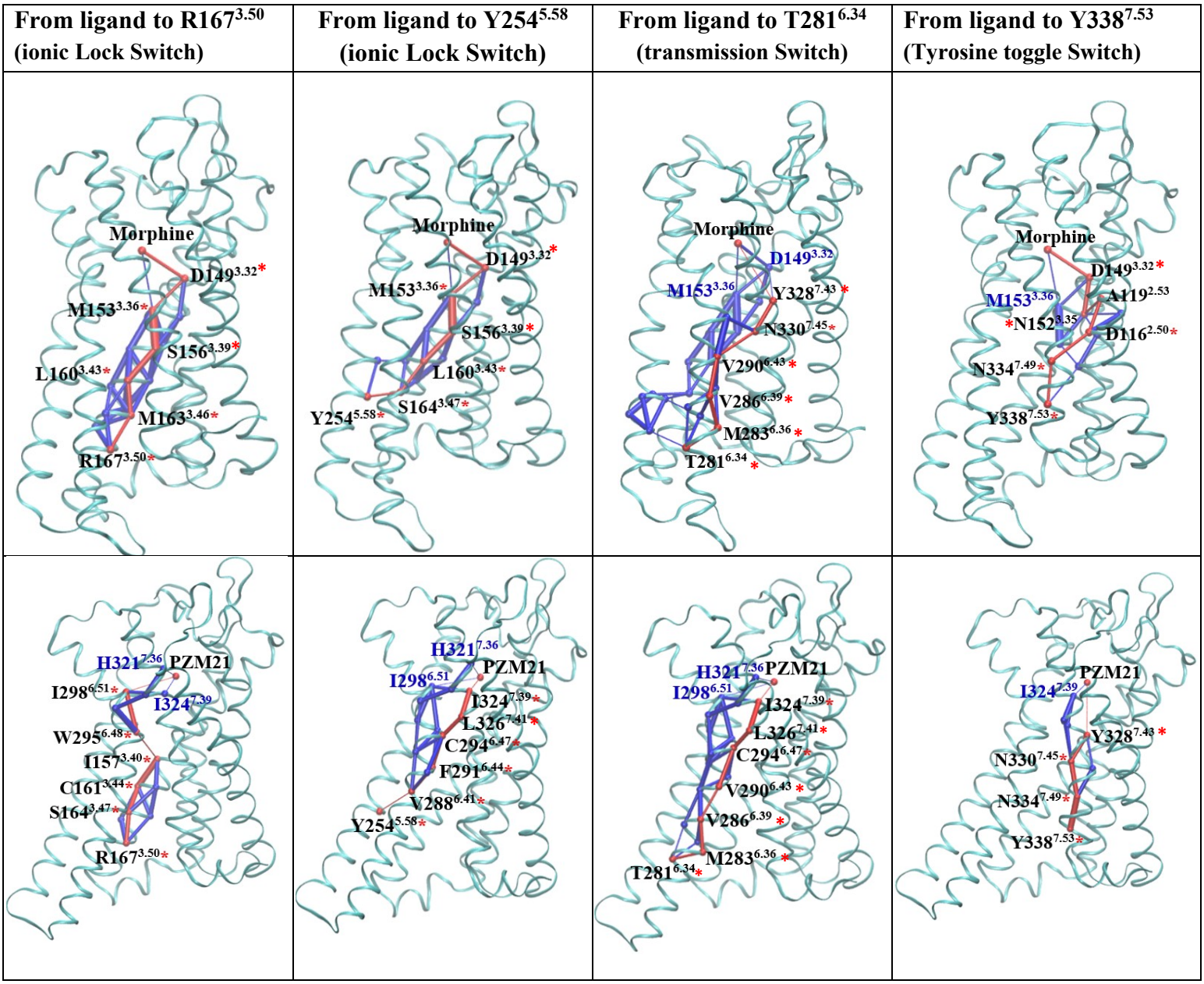

Fig. 12. The optimal (red) and suboptimal (blue) paths from the ligands to molecular switch residues of TM3 (R167$^{3.50}$), TM5 (Y254$^{5.58}$), TM6 (T281$^{6.34}$) and TM7 (Y338$^{7.53}$) during the two independent ~3.5 μs MD simulations of the morphine (top row) and PZM21 (bottom row) complex systems. The residues in optimal path (red) are labelled in black, where conserved residues are noted by red asterisks. The residues correlating with the ligands in suboptimal path (blue) are labelled in blue.

3.13. Principal component analysis (PCA) of Morphine and PZM21 systems revealed significant differences in the motions of the intracellular ends of TM5-6 and ICL3.

To further probe the overall motion of the receptor, the PCA based on the two independent ~3.5 μs MD trajectories of the Morphine and PZM21 systems was performed and generated the top five motion modes for each system in **Fig. 13**, showing that the greater fluctuation are primarily located at the intracellular ends of TM5-6, ICL3 and terminals. Especially, the modes **1** (the lowest energetic modes) showed that the intracellular ends of TM5-6 and ICL3 of the PZM21-bound MOR exhibited stronger fluctuation, due to the more directional vectors in this region. Moreover, the vivid movements of the modes **1** further clearly showed that the intracellular ends of TM5-6 and ICL3 of PZM21-bound MOR moved outward more strongly than that of Morphine-bound MOR (Movies **1** and **2**).

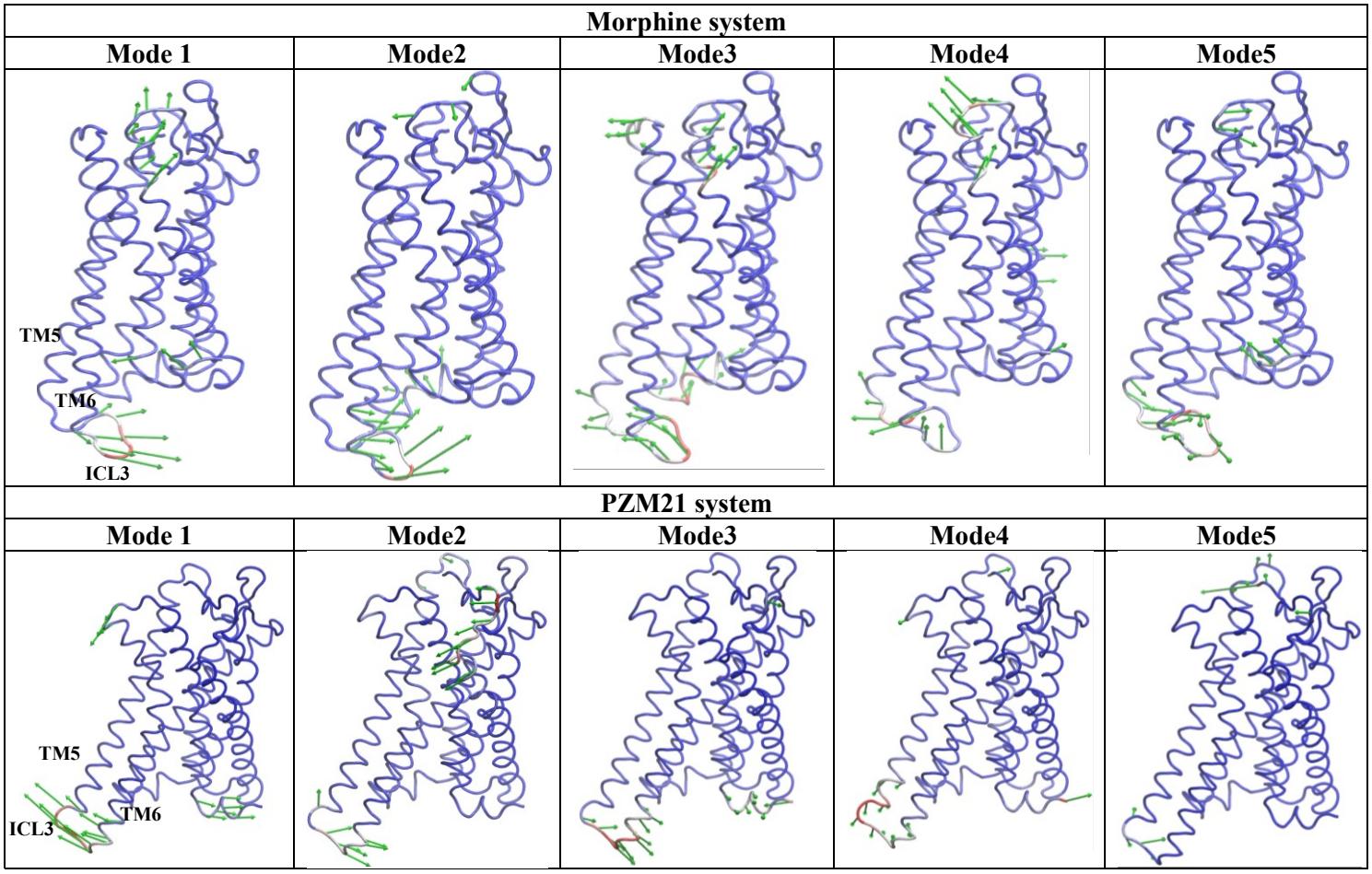

Fig. 13. The top five motion modes based on principal component analysis (PCA) performed using VMD's normal mode wizard for the two independent ~3.5 μs MD trajectories for Morphine and PZM21 systems. The color scheme is as follows: blue- low movement, grey- moderate movement, red-maximum movement. Vectors of 3.5 Å or greater are shown and represent the directionality of movement, where longer vectors represent greater fluctuations.

3.14. The interaction modes of the induced fit dockings with the crystal waters and the above Glide XP dockings without the crystal waters are similar.

In order to consider the importance of crystal waters in binding site and conformational changes in the receptor human MOR-1, the Glide XP docking and induced fit docking calculations in

presence of crystal waters were further performed to decipher more precise interactions of Morphine and PZM21 with the receptor, and the corresponding results are shown in **Fig. S20** and **Fig. S21**, respectively. Here, Morphine and PZM21 primarily form similar ionic, hydrogen-bonding and hydrophobic interactions with D149$^{3.32}$ and Y150$^{3.33}$, similar to the results of above Glide XP dockings in absence of crystal waters (**Fig. S6**), except that there are additional hydrogen-bonding interactions between hydroxyl groups of the ligands and some crystal waters. In addition, overlap of the Glide XP pose with the induced fit pose, both in presence of crystal waters, shows similar binding poses for each system (**Fig. S22**); overlap of the Glide XP docked pose in absence of crystal waters with the induced fit docked pose in presence of crystal waters shows similar scaffold orientations of binding poses for each system (**Fig. S23**). Therefore, the two ligands' interaction modes of induced fit dockings with crystal waters are respectively in good agreement with that of above Glide XP dockings without crystal waters.

3.14. The MD simulations of the two systems with the crystal waters showed similar results to the systems without the crystal waters.

The RMSD plots of the protein and ligand averaged over the two independent ~1.0 μs MD simulations are relatively flat during the last 100 ns (**Fig. S23**), indicating that each of the two systems in presence of crystal waters have reached a relatively stable state. The ligand-protein interactions for Morphine and PZM21 complexes with crystal waters during each ~1.0 μs MD simulation are shown in **Fig. S24**. In the trajectories **1** and **2**, the Morphine and PZM21 can keep forming dominant hydrogen-bonding and hydrophobic interactions with D149$^{3.32}$ and Y150$^{3.33}$, with higher interaction fractions than other residues. Of note, the PZM21 could form strong hydrogen-bond interaction with Y328$^{7.43}$, but Morphine couldn't. Indeed, the interaction modes are similar to that obtained from the above ~3.5 μs MD simulations in absence of crystal waters

(**Figs. 3-4**), except that there are stronger crystal-water mediated hydrogen bonds with K235$^{5.39}$ and H299$^{6.52}$, which potentially help to fix the ligand in the binding site to decrease the ligand's fluctuation during the MD simulations.

During the 2 runs of ~1.0 μs MD simulations, both Morphine and PZM21 adopt **three** clusters and the representative structures in each cluster are shown in **Fig. S25**. The dominant clusters of Morphine and PZM21 systems have 80.6% and 70.1% conformations, respectively. In each system, the superimposition of the three representative structures shows that the three binding poses of Morphine or PZM21 are similar, meaning that the interaction between the ligand and the receptor is relatively stable during the MD simulations. Obviously, compared with the above ~7.0 μs MD simulations, the PZM21 exhibited smaller fluctuation, likely due to the presence of the crystal waters in the binding site.

Moreover, the superimposition of each representative structure in the most abundant cluster of Morphine and PZM21 systems during the additional MD simulations also clearly illustrates the intracellular end of TM5-6 along with ICL3 of PZM21-bound MOR are stretched more outward than that of Morphine-bound MOR (**Fig. S26**). The binding conformations of Morphine and PZM21 show that the positions of their phenolic hydroxyls and tertiary amino groups are similar, respectively, which allows the tertiary amine group to interact with D149$^{3.32}$ and Y150$^{3.33}$, and the phenolic hydroxyl to interact indirectly with K235$^{5.39}$ and H299$^{6.52}$, mediated by two crystal waters. In addition, the superimpositions of the most abundant cluster's representative Morphine complexes and PZM21 complexes in two different situations (i.e., one situation includes the crystal waters but another does not), show that the two binding conformations of Morphine are similar (**Fig. S27**); the two binding conformations of PZM21 are different but with similar scaffold orientations of their phenolic hydroxyls and tertiary amino groups (**Fig. S28**). Therefore, in the

two different situations with the crystal waters or not, the preferred complex conformations of each system are, globally, similar.

3.15. The network analysis and PCA of the Morphine and PZM21 systems with the crystal waters also showed similar results to the systems without the crystal waters.

The optimal and suboptimal paths from the ligand to the molecular-switch residues in TM6-7 of the two systems with crystal waters were also analyzed (**Fig. S29**). For the signals to T281$^{6.34}$ of TM6, the optimal paths of the two systems pass through four same residues of TM6, and the Morphine's optimal path is one of the PZM21's suboptimal paths. For the signals to Y338$^{7.53}$ of TM7, Morphine's optimal path goes primarily along TM3, TM2 and TM7, whereas PZM21's goes directly along TM7. Therefore, for the two systems in presence of crystal waters, the signals to the intracellular end of TM6 are similar, but to the intracellular end of TM7 are different. The result is in good agreement with the above network analyses without crystal waters. Moreover, the PZM21's optimal paths to TM7 in the two situations (with crystal waters or not) are the same; the Morphine's suboptimal paths to TM7 with crystal waters and its suboptimal paths to TM7 without crystal waters is also the same. It could be speculated that these crystal waters likely do not play an important role in affecting the signal pathway bias.

As the result from the above PCA of Morphine and PZM21 systems without crystals waters, the top PCA Modes **1** of the two systems with crystals waters also show that PZM21-bound MOR moves outward more strongly with more vectors in this region (**Fig. S30**). This result also could be identified by the vivid movements of Modes 1 of the two systems (Movies **3** and **4**).

4. Discussion

Morphine and other opioids produce effective analgesia but accompanied by the risk of drug resistance, dependence, and other adverse effects through prolonged use. Discovering and optimizing new lead compounds that bind to opioid receptors and produce analgesia with minimized side effects are in critical need. Recently, PZM21 as a potential candidate showed effective analgesia but minimal adverse side effects. However, high resolution complex structure of a PZM21-MOR system is not yet available, so in this study we used homology modeling, molecular docking and MD simulations to probe detailed structural and dynamic insights of the PZM21-MOR system, and to present information about the preferred PZM21-bound MOR conformation and the allosteric signal transmission for G protein biased pathway.

Solution-state NMR has shown that conformational change of MOR to a fully active state (especially the TM6 outward displacement) was not related to the agonist BU72 binding alone but rather depend on the presence of both the agonist and the transducer (G protein, arrestin or their mimetic nanobody), revealing a weak allosteric coupling between the agonist-binding site and the intracellular transducer-coupling interface[71]. This loose allosteric coupling can be demonstrated by another experimental result showing that agonist-bound β_2-adrenergic receptor (β_2AR) shift the conformational equilibrium toward a conformation capable of coupling G protein, but they do so incompletely with increased conformational heterogeneity and the coexistence of inactive, intermediate and active states[72]. Like the β_2AR, the agonist-bound human A_{2A} adenosine receptor (A_{2A}AR) is also involved in both induced fit and re-equilibration of conformational ensembles [73]. In addition, the loose allosteric coupling also could be visualized in MD simulations showing that an agonist-bound β_2AR transitioned spontaneously from an active state to an inactive state on time-scales of several microseconds; and most of the receptor population remains inactive in the absence of a G protein or G protein-mimetic nanobody, although agonist

binding likely increases the fraction of active receptors[74]. All these results implied that the active state of agonist-MOR complex in absence of the transducer wasn't stable enough as its inactive state; the agonist-MOR complex coexists in multiple conformations including inactive, intermediate and active states; and the allosteric coupling was weak. Therefore, it is reasonable that the two agonist-MOR complexes in our simulations adopted active-like conformations with the hallmark outward movement of TM6[63, 66] (**Fig. 9**); the PZM21-bound MOR appeared very mobile with five conformational clusters in our MD simulations; and some of the edges in our network pathways were very thin, suggesting that they are weak links in the pathway.

The current study aims at the agonist-bound active state without G protein/arrestin/nanobody. If the simulation time is long enough, the active state would likely transition to its more stable inactive state. However, the bias activation mechanism of MOR is closely related to the active conformations of the agonist-MOR complex, thus the agonist-MOR complex here doesn't have to achieve its final inactive state during the MD simulations. Although our simulations had not achieved their final inactive state by 2 runs of ~3.5 μs, they showed the dynamics and conformations of the active-like agonist-MOR complex. Moreover, relatively flat plots of average RMSD values after 1500 ns were observed, indicating the two complex systems have achieved relatively steady states. Therefore, the timescales (~3.5 μs) of our simulations were appropriate, and the differences between morphine and PMZ21-bound MORs observed here can be used to analyze their bias activation mechanisms.

The previous studies have shown that most opioid ligands can form a salt bridge or H-bond with $D149^{3.32}$ of opioid receptors [36, 61, 62], and the results from our MD simulations identified that Morphine and PZM21 did form the critical interactions (**Fig. 3**). Moreover, residues $D149^{3.32}$, $M153^{3.36}$ and $I298^{6.51}$ were determined as crucial residues for Morphine activity by site-directed

mutagenesis study[75], and these residues were also involved in Morphine's interactions from our MD simulations (**Fig. 4**). Therefore, our calculation results from the homology modeling, Glide XP docking and MD simulations are credible.

The MD simulations of the two systems uncovered specific receptor conformations and ligand-protein interactions. The key residues $D149^{3.32}$ and $Y150^{3.33}$ of TM3 are conserved in both Morphine and PZM21 systems and comprise the strongest and most prevelant interactions (**Fig. 4**), indicating the interactions with $D149^{3.32}$ and $Y150^{3.33}$ are crucial for the activation of MOR. However, compared with the compact rigid structure Morphine, the elongated structure PZM21 was exhibited greater fluctuation and flexibility with greater ligand RMSD (**Fig. 2**) and RMSF values (**Fig. 8**). As a result, the interaction mode of PZM21 showed slightly different from that of Morphine, i.e., PZM21 has strong interactions with $Y328^{7.43}$ of TM7 (**Fig. 4**). This difference in ligand-binding modes would potentially affect their allosteric networks involved in the receptor's activation signaling pathways.

The dynamics of PZM21 and Morphine in complex with MOR were different from each other during our MD simulations. First, PZM21-MOR complex adopted more conformational clusters than Morphine-MOR complex (**Fig. S14**), meaning that the active states of PZM21-MOR complex exhibited stronger fluctuation. Second, the most notable conformational change of the receptor in the PZM21-MOR complex was located at the intracellular ends of TM5-7 being bent outwards and creating a wider opening (**Fig. S11**). Meanwhile, the two systems are also shown some differences at TM5-7 from the protein SSE analyses (**Fig. 6**). In addition, PZM21-bound MOR exhibited larger fluctuations at TM5-6 from the protein RMSF data (**Fig. 7**). These different TM5-7 changes in the two systems might be correlative with their molecular switches, so it was very necessary to carry out molecular switches analyses.

The representative structures of the most abundant clusters in the two systems further verified that the active MOR structures appeared some common characters of active GPCR structures, including TM5 bending toward TM6, TM6 bending outward, and TM7 bending inward (**Fig. 9**). The larger differences in the two systems appeared at the ionic lock, transmission and Tyr toggle switches, and PZM21-activated MOR showed more obvious outward movement of TM6 intercellular end, rotation of $W295^{6.48}$, and inward movement of $Y388^{7.53}$. Moreover, the distances of these molecular switches throughout our MD simulations were further measured. As anticipated, the average distances of ionic lock and Tyr toggle switches of PZM21 systems were longer than that of Morphine system, but the average distances of transmission switch was shorter , especially in the last 500 ns (**Fig. S13**). As a result, PZM21-bound MOR's TM5-6 helices were bent outward more, but its TM7 was bent inward less. Simultaneously, the movements of the lowest energetic PCA modes (Modes **1**) clearly showed that the intracellular ends of TM5-6 and ICL3 of PZM21-bound MOR bent outward more strongly than that of Morphine-bound MOR (**Fig. 13 and Movies 1 and 2**). In addition, the geometric center distances of the **34** conserved residue pairs throughout our MD simulations are shown that the distances of the five conserved inter-helical residue pairs in PZM21 system increased when compared with Morphine system (**Fig. 10**). So that the PZM21 system would decrease the contacts among TMs and easily cause the outward movements of TMs, potentially leading to the appearance of the larger cavity at the intracellular end of PZM21-bound MOR (**Fig. 9**). Therefore, an observed feature of human MOR activation from our MD simulations is a greater opening of the intracellular end for the PZM21-bound MOR, which will facilitate G protein binding. The result is in good agreement with the previous NMR result revealing that the intracellular cavity of MOR coupled with Morphine or another biased agonist TRV130 existed in an equilibrium between closed and multiple open conformations, and

the equilibrium within the open conformations of TRV130-bound MOR were shifted toward the conformations with a larger intracellular cavity than that of Morphine-bound MOR[27].

Based on ^{19}F-NMR signals, Liu *et al.* observed that unbiased agonists affected the conformational states of TM6 and TM7 in β_2AR, and β-arrestin-biased ligands predominantly impact the conformational states of TM7[70]. Similarly, Rahmeh *et al*. proposed that the signal pathways of biased ligands depend on the effect they trigger in the TM6 (G_S protein pathway) and TM7-H8 (arrestin pathway). They used two fluorescence-based approaches to study the arginine-vasopressin type 2 receptor (V2R), showing that the unbiased agonist natural hormone arginine-vasopressin (AVP, Gs agonist and β-arrestin agonist) able to activate the two signaling pathways by triggering TM6 and TM7-H8 domains, but the biased agonist MCF14 (G_s agonist and arrestin antagonist) is only able to trigger the TM6 domain [76]. Particularly, the degree of the outward movement of TM6 in arrestin-bound rhodopsin is smaller than that in G protein-bound β2AR, suggesting that arrestin recognizes a GPCR that exhibits a relatively small outward movement of TM6 [77]. Although our MD simulations of the two systems showed large outward movement of TM6 and inward movement of TM7 in comparison with the inactive MOR structure, the intracellular TM6 of PZM21-bound MOR moved outward more than that of Morphine-bound MOR, and the intracellular TM7 of Morphine-bound MOR moved inward more than that of PZM21-bound MOR (**Fig. 9**). It is known that molecular movements as small as 1Å can lead to profound modifications on the activity of receptors[78]. Therefore, according to the different conformational changes of TM6 and TM7, it can be speculated that the PZM21 system with larger outward movement of TM6 may be more favorable to activate G protein pathway than Morphine system, and the Morphine system, with smaller outward movement of TM6 and larger inward movement of TM7, may be more favorable to activate arrestin pathway than PZM21 system.

Of note, the biased signaling mechanisms of GPCRs are very complex and the result of many aspects. In our MD simulations, we clearly observed the increased opening of the intracellular interface, which can potentially facilitate G protein binding. But that doesn't mean that other factors can be ruled out, such as decreased arrestin-binding, which closely connects with efficiency of phosphorylation of C-terminal tail, interaction of arrestin to the phosphorylated C terminus, efficiency of receptor sorting into endosomes, etc.[79-81], even though some of these mechanisms affecting arrestin-binding were not analyzed in our MD simulations due to PZM21 being a G protein agonist. In this paper, owing to time and calculation limitations, we simulated only one unbiased agonist (Morphine) vs. G protein biased agonist (PZM21). As observed from the previous MD simulations, another G-protein biased agonist TRV130 showed that the strong stabilization of $W^{6.48}$ by interacting with $Y^{7.43}$ is useful for its G protein-biased signaling pathway [26]. Interestingly, our critical node analysis also implied that the two residues were closely associated with its biased pathway. To better understand the biased signaling mechanisms of MOR, it is necessary to compare the dynamics of multiple unbiased agonists vs. G protein agonists to reveal more convincing information for designing the ligand with G protein bias, which is necessary to be performed in the future.

The different TM5-7 conformation changes in the two systems might be correlative with their specific loose allosteric interactions, so it was very necessary to carry out networks analyses. The conserved critical nodes are responsible for the signal communication between different network communities and play a critical role in signal transduction (**Table 1**). The common conserved residues may be important for the G protein signal transduction, whereas the other different residues may influence the signal pathway bias. Out of **9** common conserved critical nodes, interestingly, the residues $L160^{3.43}$ and $F291^{6.44}$ are the key residues of the hydrophobic hindering

mechanism core (HHM core, composed primarily of $F^{6.44}$, $L^{3.43}$ and $X^{6.40}$, in addition to $L^{2.46}$, $N^{7.49}$, $Y^{7.53}$, $Y^{5.58}$, $R^{3.50}$ and $X^{6.41}$) involved in the activation process from orthosteric site to G protein docking site for all family A GPCRs seen to date[67]. Therefore the importance of $L160^{3.43}$ and $F291^{6.44}$ in the signaling of G protein pathway could be deduced. Moreover, among the conserved critical nodes of Morphine system, the **3** residues $I157^{3.40}$, $P246^{5.50}$ and $F291^{6.44}$ form the conserved core triad[36], and the **4** residues $L160^{3.43}$, $F291^{6.44}$, $Y254^{5.58}$ and $N334^{7.49}$ belong to the HHM core[67]. On the other hand, among the conserved critical nodes of PMZ21 system, the **2** residues $I157^{3.40}$ and $F291^{6.44}$ belong to the conserved core triad, the **7** residues $F291^{6.44}$, $L160^{3.43}$, $V287^{6.40}$, $L112^{2.46}$, $Y338^{7.53}$, $R167^{3.50}$ and $V288^{6.41}$form the HHM core, and the $W295^{6.48}$ belong to transmission switch. Compared with the two systems, it is clear that the PZM21 system has more residues associated with switch motifs, especially associated with the HHM core that is very important for the activation of G protein process for class A GPCRs[67]. Therefore, the PZM21 system may be more preferred to activate G pathway than the Morphine system.

The different critical nodes in the two systems may be associated with the signal pathway bias (**Table 1**). A previous experimental study showed that the mutations $W320^{7.35}$A and $Y328^{7.43}$F of MOR caused changes in pathway bias, with different patterns among different ligands [82]. In addition, a previous computational study showed that the strong stabilization of $W^{6.48}$ by interacting with $Y^{7.43}$ is useful for the G protein-biased activation of TRV130-MOR system [26]. Interestingly, three critical nodes $W^{6.48}$, $W320^{7.35}$ and $Y328^{7.43}$ in PZM21 system may be associated with PZM21's G protein-biased pathway. Similarly, the two critical nodes $N152^{3.35}$ and $F158^{3.41}$ in Morphine system may influence the β-arrestin-biased pathway, which is also consistent with the experimental result showing that the mutations $N152^{3.35}$A and $F158^{3.41}$W of MOR caused a significant increase of β-arrestin-mediated signaling for ligand TRV130[27]. Therefore, some

critical nodes in our network analyses definitely played a significant role in signal transduction and reasonably explained some experimental results.

Moreover, for the unbiased agonist Morphine and the biased agonist PZM21, their network paths from the ligand to the molecular switches were slightly different (**Fig. 12**). On one hand, the network paths to the intracellular ends of the three TMs (TM3, TM5 and TM7) are different between the two systems, but the two systems' optimal paths to the transmission switch in the intracellular end of TM6 were similar. On the other hand, the network signals from PZM21 to the molecular switches of TM3, TM5 and TM7 with some thinner edges were a little bit weaker than that from Morphine. Interestingly, out of the **5** residues ($D149^{3.32}$, $N152^{3.35}$, $A119^{2.53}$, $D116^{2.50}$ and $N334^{7.49}$) in the optimal path to the $Y338^{7.53}$ of TM7 in Morphine system (**Fig. 12**), the **3** residues $D^{2.50}$, $N^{3.35}$ and $N^{7.49}$ were shown to increase the β-arrestin-mediated signaling by the mutations of $N^{3.35}$A or V, $D^{2.50}$A, $N^{7.49}$A for δ-opioid receptor[83]. Therefore, our optimal and suboptimal paths are able to reasonably explain the experimental results. In addition, like the network paths from the ligand to the molecular switches of TM6-7, the paths from the key contact residues $D149^{3.32}$ and $Y150^{3.33}$ to the end of TM6 were also similar in the two systems, but the paths to the end of TM7 were different (**Fig. S19**). It is known that the conformation of TM6 is related to the efficiency of G protein coupling and the conformation of TM7 is related to the efficiency of arrestin coupling[70]. Therefore, it is possible that both Morphine and PZM21 can trigger the G protein pathway activation due to their network paths to TM6 being similar, while Morphine is more favorable to couple arrestin than PZM21 due to its network paths to TM7 being different and relatively stronger (with thicker edges).

The results about these additional induced fit docking, 2 runs of ~1.0 μs MD simulations, network analysis and PCA of the two complex systems in presence of the crystal waters are

respectively similar to that in absence of the crystal waters (**Figs**. **S20**-**S30**). These further confirm that the results obtained from the systems without the crystal waters are reasonable and credible. Simultaneously, it could be speculated that the crystal waters in the binding site may not play a key role in affecting the signal pathway bias of PZM21, although they likely improve the stability of PZM21 during the MD simulations.

5. Conclusion

Based on our MD simulations in two different situations (i.e., one situation includes the crystal waters but another does not), some valuable information about G protein biased signaling pathways of PZM21-MOR complex was revealed as follows: (1) PZM21 could interact with $Y328^{7.43}$ of TM7, besides the key residues $D149^{3.32}$ and $Y150^{3.33}$ of TM3. (2) Morphine and PZM21 systems' network paths to the intracellular end of TM6 were roughly similar but the paths to the end of TM7 were clearly distinct. (3) Accompanied by the distance changes of the three key molecular switches (ionic lock, transmission and Tyr toggle) and the distance increase of some conserved inter-helical residue pairs, PZM21-bound MOR exhibited larger outward movement of TM5-6 and less inward movement of TM7. (4) The PZM21-bound MOR's intracellular ends of TM5-7 bent outward more and created a larger cavity potentially favorable for G protein binding.

Conflicts of interest

All of the authors declare no conflicts of interest.

Acknowledgements

This work was supported by Rowan University CSM SEED fund and the National Science Foundation of USA under Grant RUI-1904797. We also acknowledge the High Performance Computing Facility at Rowan funded by the National Science Foundation of USA under Grant MRI-1429467 and XSEDE MCB160164/160173/170088. The Anton2 machine at the Pittsburgh Supercomputing Center (MCB170090P) was generously made available by D. E. Shaw Research.

References

[1] J.C. Ballantyne, J. Mao, Opioid therapy for chronic pain, N. Engl. J. Med., 349 (2003) 1943-1953.
[2] H. McQuay, A. Moore, D. Justins, Treating acute pain in hospital, BMJ, 314 (1997) 1531-1535.
[3] M.D. Sullivan, C.Q. Howe, Opioid therapy for chronic pain in the United States: promises and perils, Pain, 154 Suppl 1 (2013) S94-100.
[4] G.W. Pasternak, Opiate pharmacology and relief of pain, J. Clin. Oncol., 32 (2014) 1655-1661.
[5] A. Madariaga-Mazon, A.F. Marmolejo-Valencia, Y.M. Li, L. Toll, R.A. Houghten, K. Martinez-Mayorga, Mu-Opioid receptor biased ligands: A safer and painless discovery of analgesics?, Drug Discovery Today, 22 (2017) 1719-1729.
[6] A.D. Corbett, G. Henderson, A.T. McKnight, S.J. Paterson, 75 years of opioid research: the exciting but vain quest for the Holy Grail, British Journal of Pharmacology, 147 (2006) S153-S162.
[7] M. Waldhoer, S.E. Bartlett, J.L. Whistler, Opioid receptors, Annual Review of Biochemistry, 73 (2004) 953-990.
[8] B. Trzaskowski, D. Latek, S. Yuan, U. Ghoshdastider, A. Debinski, S. Filipek, Action of Molecular Switches in GPCRs - Theoretical and Experimental Studies, Current Medicinal Chemistry, 19 (2012) 1090-1109.
[9] E.R. Siuda, R. Carr, D.H. Rominger, J.D. Violin, Biased mu-opioid receptor ligands: a promising new generation of pain therapeutics, Current Opinion in Pharmacology, 32 (2017) 77-84.
[10] D. Liao, H. Lin, P.Y. Law, H.H. Loh, Mu-opioid receptors modulate the stability of dendritic spines, Proceedings of the National Academy of Sciences of the United States of America, 102 (2005) 1725-1730.
[11] Z.Y. Zuo, The role of opioid receptor internalization and beta-arrestins in the development of opioid tolerance, Anesthesia and Analgesia, 101 (2005) 728-734.
[12] L.M. Bohn, R.J. Lefkowitz, M.G. Caron, Differential mechanisms of morphine antinociceptive tolerance revealed in beta arrestin-2 knock-out mice, Journal of Neuroscience, 22 (2002) 10494-10500.
[13] K.M. Raehal, J.K.L. Walker, L.M. Bohn, Morphine side effects in beta-arrestin 2 knockout mice, Journal of Pharmacology and Experimental Therapeutics, 314 (2005) 1195-1201.
[14] C.E. Groer, K. Tidgewell, R.A. Moyer, W.W. Harding, R.B. Rothman, T.E. Prisinzano, L.M. Bohn, An opioid agonist that does not induce mu-opioid receptor--arrestin interactions or receptor internalization, Mol Pharmacol, 71 (2007) 549-557.
[15] S.M. DeWire, D.S. Yamashita, D.H. Rominger, G.D. Liu, C.L. Cowan, T.M. Graczyk, X.T. Chen, P.M. Pitis, D. Gotchev, C. Yuan, M. Koblish, M.W. Lark, J.D. Violin, A G Protein-Biased Ligand at the mu-Opioid Receptor Is Potently Analgesic with Reduced Gastrointestinal and Respiratory Dysfunction Compared

with Morphines, Journal of Pharmacology and Experimental Therapeutics, 344 (2013) 708-717.
[16] N. Singla, H.S. Minkowitz, D.G. Soergel, D.A. Burt, R.A. Subach, M.Y. Salamea, M.J. Fossler, F. Skobieranda, A randomized, Phase IIb study investigating oliceridine (TRV130), a novel micro-receptor G-protein pathway selective (mu-GPS) modulator, for the management of moderate to severe acute pain following abdominoplasty, J Pain Res, 10 (2017) 2413-2424.
[17] A. Manglik, H. Lin, D.K. Aryal, J.D. McCorvy, D. Dengler, G. Corder, A. Levit, R.C. Kling, V. Bernat, H. Hubner, X.P. Huang, M.F. Sassano, P.M. Giguere, S. Lober, D. Duan, G. Scherrer, B.K. Kobilka, P. Gmeiner, B.L. Roth, B.K. Shoichet, Structure-based discovery of opioid analgesics with reduced side effects, Nature, 537 (2016) 185-190.
[18] S. Bharadwaj, K.E. Lee, V.D. Dwivedi, S.G. Kang, Computational insights into tetracyclines as inhibitors against SARS-CoV-2 M-pro via combinatorial molecular simulation calculations, Life Sci., 257 (2020).
[19] S.Y. Liao, C. Floyd, N. Verratti, L. Leung, C. Wu, Analysis of vismodegib resistance in D473G and W535L mutants of SMO receptor and design of novel drug derivatives using molecular dynamics simulations, Life Sci., 244 (2020).
[20] M.S. Liu, G.Z. Liang, H.L. Zheng, N. Zheng, H. Ge, W.D. Liu, Triazoles bind the C-terminal domain of SMO: Illustration by docking and molecular dynamics simulations the binding between SMO and triazoles, Life Sci., 217 (2019) 222-228.
[21] N. Rasafar, A. Barzegar, E.M. Aghdam, Design and development of high affinity dual anticancer peptide-inhibitors against p53-MDM2/X interaction, Life Sci., 245 (2020).
[22] A.I. Uba, C. Radicella, C. Readmond, N. Scorese, S.Y. Liao, H.G. Liu, C. Wu, Binding of agonist WAY-267,464 and antagonist WAY-methylated to oxytocin receptor probed by all-atom molecular dynamics simulations, Life Sci., 252 (2020).
[23] A. Rohini, N. Agrawal, H. Kumar, V. Nath, V. Kumar, Norbixin, an apocarotenoid derivative activates PPAR gamma in cardiometabolic syndrome: Validation by in silico and in vivo experimental assessment, Life Sci., 209 (2018) 69-77.
[24] S. Schneider, D. Provasi, M. Filizola, How Oliceridine (TRV-130) Binds and Stabilizes a μ-Opioid Receptor Conformational State That Selectively Triggers G Protein Signaling Pathways, Biochemistry, 55 (2016) 6456-6466.
[25] J. Ballesteros, H. Weinstein, Integrated methods for the construction of three-dimensional models and computational probing of structure-function relations in G protein-coupled receptors, Methods in Neurosciences, 25 (1995) 366-428.
[26] J.X. Cheng, T. Cheng, W.H. Li, G.X. Liu, W.L. Zhu, Y. Tang, Computational insights into the G-protein-biased activation and inactivation mechanisms of the mu opioid receptor, Acta Pharmacol Sin, 39 (2018) 154-164.
[27] J. Okude, T. Ueda, Y. Kofuku, M. Sato, N. Nobuyama, K. Kondo, Y. Shiraishi, T. Mizumura, K. Onishi, M. Natsume, M. Maeda, H. Tsujishita, T. Kuranaga, M. Inoue, I. Shimada, Identification of a Conformational Equilibrium That Determines the Efficacy and Functional Selectivity of the mu-Opioid Receptor, Angew Chem Int Ed Engl, 54 (2015) 15771-15776.
[28] M.A. Lomize, I.D. Pogozheva, H. Joo, H.I. Mosberg, A.L. Lomize, OPM database and PPM web server: resources for positioning of proteins in membranes, Nucleic Acids Research, 40 (2012) D370-D376.
[29] E. Harder, W. Damm, J. Maple, C. Wu, M. Reboul, J.Y. Xiang, L. Wang, D. Lupyan, M.K. Dahlgren, J.L. Knight, J.W. Kaus, D.S. Cerutti, G. Krilov, W.L. Jorgensen, R. Abel, R.A. Friesner, OPLS3: A Force Field Providing Broad Coverage of Drug-like Small Molecules and Proteins, Journal of Chemical Theory and Computation, 12 (2016) 281-296.
[30] G.M. Sastry, M. Adzhigirey, T. Day, R. Annabhimoju, W. Sherman, Protein and ligand preparation: parameters, protocols, and influence on virtual screening enrichments, J Comput Aided Mol Des, 27 (2013) 221-234.

[31] M.P. Jacobson, D.L. Pincus, C.S. Rapp, T.J.F. Day, B. Honig, D.E. Shaw, R.A. Friesner, A hierarchical approach to all-atom protein loop prediction, Proteins-Structure Function and Bioinformatics, 55 (2004) 351-367.
[32] M.P. Jacobson, R.A. Friesner, Z. Xiang, B. Honig, On the Role of the Crystal Environment in Determining Protein Side-chain Conformations, Journal of Molecular Biology, 320 (2002) 597-608.
[33] M. Magrane, C. UniProt, UniProt Knowledgebase: a hub of integrated protein data, Database-the Journal of Biological Databases and Curation, (2011).
[34] R.A. Friesner, R.B. Murphy, M.P. Repasky, L.L. Frye, J.R. Greenwood, T.A. Halgren, P.C. Sanschagrin, D.T. Mainz, Extra precision glide: Docking and scoring incorporating a model of hydrophobic enclosure for protein-ligand complexes, Journal of Medicinal Chemistry, 49 (2006) 6177-6196.
[35] R.A. Friesner, J.L. Banks, R.B. Murphy, T.A. Halgren, J.J. Klicic, D.T. Mainz, M.P. Repasky, E.H. Knoll, M. Shelley, J.K. Perry, D.E. Shaw, P. Francis, P.S. Shenkin, Glide: A new approach for rapid, accurate docking and scoring. 1. Method and assessment of docking accuracy, Journal of Medicinal Chemistry, 47 (2004) 1739-1749.
[36] W. Huang, A. Manglik, A.J. Venkatakrishnan, T. Laeremans, E.N. Feinberg, A.L. Sanborn, H.E. Kato, K.E. Livingston, T.S. Thorsen, R.C. Kling, S. Granier, P. Gmeiner, S.M. Husbands, J.R. Traynor, W.I. Weis, J. Steyaert, R.O. Dror, B.K. Kobilka, Structural insights into micro-opioid receptor activation, Nature, 524 (2015) 315-321.
[37] W. Sherman, T. Day, M.P. Jacobson, R.A. Friesner, R. Farid, Novel procedure for modeling ligand/receptor induced fit effects, Journal of Medicinal Chemistry, 49 (2006) 534-553.
[38] W.L. Jorgensen, D.S. Maxwell, J. TiradoRives, Development and testing of the OPLS all-atom force field on conformational energetics and properties of organic liquids, Journal of the American Chemical Society, 118 (1996) 11225-11236.
[39] D. Shivakumar, J. Williams, Y.J. Wu, W. Damm, J. Shelley, W. Sherman, Prediction of Absolute Solvation Free Energies using Molecular Dynamics Free Energy Perturbation and the OPLS Force Field, Journal of Chemical Theory and Computation, 6 (2010) 1509-1519.
[40] E. Lyman, C. Higgs, B. Kim, D. Lupyan, J.C. Shelleys, R. Farid, G.A. Voth, A Role for a Specific Cholesterol Interaction in Stabilizing the Apo Configuration of the Human A(2A) Adenosine Receptor, Structure, 17 (2009) 1660-1668.
[41] P. Mark, L. Nilsson, Structure and dynamics of the TIP3P, SPC, and SPC/E water models at 298 K, Journal of Physical Chemistry A, 105 (2001) 9954-9960.
[42] J. Zhang, Y. Hou, Y. Wang, C. Wang, X. Zhang, The LBFGS quasi-Newtonian method for molecular modeling prion AGAAAAGA amyloid fibrils, Natural Science, 04 (2012) 1097-1108.
[43] A.G. Bailey, C.P. Lowe, MILCH SHAKE: An Efficient Method for Constraint Dynamics Applied to Alkanes, Journal of Computational Chemistry, 30 (2009) 2485-2493.
[44] Y.B. Shan, J.L. Klepeis, M.P. Eastwood, R.O. Dror, D.E. Shaw, Gaussian split Ewald: A fast Ewald mesh method for molecular simulation, Journal of Chemical Physics, 122 (2005).
[45] S.J. Stuart, R.H. Zhou, B.J. Berne, Molecular dynamics with multiple time scales: The selection of efficient reference system propagators, Journal of Chemical Physics, 105 (1996) 1426-1436.
[46] K.J. Bowers, D.E. Chow, H. Xu, R.O. Dror, M.P. Eastwood, B.A. Gregersen, J.L. Klepeis, I. Kolossvary, M.A. Moraes, F.D. Sacerdoti, J.K. Salmon, Y. Shan, D.E. Shaw, Scalable Algorithms for Molecular Dynamics Simulations on Commodity Clusters, Scalable Algorithms for Molecular Dynamics Simulations on Commodity Clusters. Proceedings of the 2006 ACM/IEEE Conference on Supercomputing, 2006 ACM/IEEE Conference on Supercomputing, pp. 43.
[47] S. El-Gebali, J. Mistry, A. Bateman, S.R. Eddy, A. Luciani, S.C. Potter, M. Qureshi, L.J. Richardson, G.A. Salazar, A. Smart, E.L.L. Sonnhammer, L. Hirsh, L. Paladin, D. Piovesan, S.C.E. Tosatto, R.D. Finn, The Pfam protein families database in 2019, Nucleic Acids Res, 47 (2019) D427-D432.
[48] A.M. Waterhouse, J.B. Procter, D.M. Martin, M. Clamp, G.J. Barton, Jalview Version 2--a multiple

sequence alignment editor and analysis workbench, Bioinformatics, 25 (2009) 1189-1191.
[49] A. Sethi, J. Eargle, A.A. Black, Z. Luthey-Schulten, Dynamical networks in tRNA:protein complexes, Proc Natl Acad Sci U S A, 106 (2009) 6620-6625.
[50] A. Black Pyrkosz, J. Eargle, A. Sethi, Z. Luthey-Schulten, Exit strategies for charged tRNA from GluRS, J Mol Biol, 397 (2010) 1350-1371.
[51] A.T. Vanwart, J. Eargle, Z. Luthey-Schulten, R.E. Amaro, Exploring residue component contributions to dynamical network models of allostery, J Chem Theory Comput, 8 (2012) 2949-2961.
[52] J. Eargle, Z. Luthey-Schulten, NetworkView: 3D display and analysis of protein.RNA interaction networks, Bioinformatics, 28 (2012) 3000-3001.
[53] J. Eargle, Z. Luthey-Schulten, NetworkView: 3D display and analysis of protein·RNA interaction networks, Bioinformatics (Oxford, England), 28 (2012) 3000-3001.
[54] W. Humphrey, Dalke, A. and Schulten, K, "VMD - Visual Molecular Dynamics", J. Molec. Graphics, 14 (1996) 33-38.
[55] N.M. Glykos, Software news and updates. Carma: a molecular dynamics analysis program, Journal of computational chemistry, 27 (2006) 1765-1768.
[56] M. Girvan, M.E.J. Newman, Community structure in social and biological networks, Proceedings of the National Academy of Sciences, 99 (2002) 7821.
[57] E.C. Dykeman, O.F. Sankey, Normal mode analysis and applications in biological physics, J Phys Condens Matter, 22 (2010) 423202.
[58] A. Bakan, L.M. Meireles, I. Bahar, ProDy: protein dynamics inferred from theory and experiments, Bioinformatics, 27 (2011) 1575-1577.
[59] I.T. Jolliffe, J. Cadima, Principal component analysis: a review and recent developments, Philos Trans A Math Phys Eng Sci, 374 (2016) 20150202.
[60] S. Sader, K. Anant, C. Wu, To probe interaction of morphine and IBNtxA with 7TM and 6TM variants of the human mu-opioid receptor using all-atom molecular dynamics simulations with an explicit membrane, Phys Chem Chem Phys, 20 (2018) 1724-1741.
[61] H.X. Wu, D. Wacker, M. Mileni, V. Katritch, G.W. Han, E. Vardy, W. Liu, A.A. Thompson, X.P. Huang, F.I. Carroll, S.W. Mascarella, R.B. Westkaemper, P.D. Mosier, B.L. Roth, V. Cherezov, R.C. Stevens, Structure of the human kappa-opioid receptor in complex with JDTic, Nature, 485 (2012) 327-332.
[62] S. Granier, A. Manglik, A.C. Kruse, T.S. Kobilka, F.S. Thian, W.I. Weis, B.K. Kobilka, Structure of the delta-opioid receptor bound to naltrindole, Nature, 485 (2012) 400-404.
[63] A. Manglik, A.C. Kruse, Structural Basis for G Protein-Coupled Receptor Activation, Biochemistry, 56 (2017) 5628-5634.
[64] W.H. Weng, Y.T. Li, H.J. Hsu, Activation-Induced Conformational Changes of Dopamine D3 Receptor Promote the Formation of the Internal Water Channel, Scientific reports, 7 (2017) 12792.
[65] V. Katritch, V. Cherezov, R.C. Stevens, Structure-Function of the G Protein-Coupled Receptor Superfamily, Annual Review of Pharmacology and Toxicology2013, pp. 531-556.
[66] Q. Zhou, D. Yang, M. Wu, Y. Guo, W. Guo, L. Zhong, X. Cai, A. Dai, W. Jang, E.I. Shakhnovich, Z.J. Liu, R.C. Stevens, N.A. Lambert, M.M. Babu, M.W. Wang, S. Zhao, Common activation mechanism of class A GPCRs, Elife, 8 (2019).
[67] B.G. Tehan, A. Bortolato, F.E. Blaney, M.P. Weir, J.S. Mason, Unifying family A GPCR theories of activation, Pharmacol Ther, 143 (2014) 51-60.
[68] A.J. Venkatakrishnan, X. Deupi, G. Lebon, C.G. Tate, G.F. Schertler, M.M. Babu, Molecular signatures of G-protein-coupled receptors, Nature, 494 (2013) 185-194.
[69] G.M. Suel, S.W. Lockless, M.A. Wall, R. Ranganathan, Evolutionarily conserved networks of residues mediate allosteric communication in proteins, Nat Struct Biol, 10 (2003) 59-69.
[70] J.J. Liu, R. Horst, V. Katritch, R.C. Stevens, K. Wuthrich, Biased Signaling Pathways in beta(2)-Adrenergic Receptor Characterized by F-19-NMR, Science, 335 (2012) 1106-1110.

[71] R. Sounier, C. Mas, J. Steyaert, T. Laeremans, A. Manglik, W. Huang, B.K. Kobilka, H. Demene, S. Granier, Propagation of conformational changes during mu-opioid receptor activation, Nature, 524 (2015) 375-378.
[72] A. Manglik, T.H. Kim, M. Masureel, C. Altenbach, Z. Yang, D. Hilger, M.T. Lerch, T.S. Kobilka, F.S. Thian, W.L. Hubbell, R.S. Prosser, B.K. Kobilka, Structural Insights into the Dynamic Process of beta2-Adrenergic Receptor Signaling, Cell, 161 (2015) 1101-1111.
[73] L. Susac, M.T. Eddy, T. Didenko, R.C. Stevens, K. Wuthrich, A2A adenosine receptor functional states characterized by (19)F-NMR, Proc Natl Acad Sci U S A, 115 (2018) 12733-12738.
[74] R.O. Dror, D.H. Arlow, P. Maragakis, T.J. Mildorf, A.C. Pan, H. Xu, D.W. Borhani, D.E. Shaw, Activation mechanism of the beta2-adrenergic receptor, Proc Natl Acad Sci U S A, 108 (2011) 18684-18689.
[75] A.W.R. Serohijos, S. Yin, F. Ding, J. Gauthier, D.G. Gibson, W. Maixner, N.V. Dokholyan, L. Diatchenko, Structural Basis for mu-Opioid Receptor Binding and Activation, Structure, 19 (2011) 1683-1690.
[76] R. Rahmeh, M. Damian, M. Cottet, H. Orcel, C. Mendre, T. Durroux, K.S. Sharma, G. Durand, B. Pucci, E. Trinquet, J.M. Zwier, X. Deupi, P. Bron, J.L. Baneres, B. Mouillac, S. Granier, Structural insights into biased G protein-coupled receptor signaling revealed by fluorescence spectroscopy, Proc Natl Acad Sci U S A, 109 (2012) 6733-6738.
[77] Y. Shiraishi, M. Natsume, Y. Kofuku, S. Imai, K. Nakata, T. Mizukoshi, T. Ueda, H. Iwai, I. Shimada, Phosphorylation-induced conformation of beta2-adrenoceptor related to arrestin recruitment revealed by NMR, Nat Commun, 9 (2018) 194.
[78] D.E. Koshland, Conformational changes: How small is big enough?, Nature Medicine, 4 (1998) 1112-1114.
[79] H.C.S. Chan, D. McCarthy, J.I. Li, K. Palczewski, S.G. Yuan, Designing Safer Analgesics via mu-Opioid Receptor Pathways, Trends in Pharmacological Sciences, 38 (2017) 1016-1037.
[80] D.P. Staus, H. Hu, M.J. Robertson, A.L.W. Kleinhenz, L.M. Wingler, W.D. Capel, N.R. Latorraca, R.J. Lefkowitz, G. Skiniotis, Structure of the M2 muscarinic receptor-beta-arrestin complex in a lipid nanodisc, Nature, 579 (2020) 297-302.
[81] W.I. Weis, B.K. Kobilka, The Molecular Basis of G Protein-Coupled Receptor Activation, Annu Rev Biochem, 87 (2018) 897-919.
[82] J.D. Hothersall, R. Torella, S. Humphreys, M. Hooley, A. Brown, G. McMurray, S.A. Nickolls, Residues W320 and Y328 within the binding site of the mu-opioid receptor influence opiate ligand bias, Neuropharmacology, 118 (2017) 46-58.
[83] G. Fenalti, P.M. Giguere, V. Katritch, X.P. Huang, A.A. Thompson, V. Cherezov, B.L. Roth, R.C. Stevens, Molecular control of delta-opioid receptor signalling, Nature, 506 (2014) 191-196.